

# Trend Filtering on Graphs

Yu-Xiang Wang<sup>1</sup>  
yuxiangw@cs.cmu.edu

James Sharpnack<sup>3</sup>  
jsharpna@gmail.com

Alex Smola<sup>1,4</sup>  
alex@smola.org

Ryan J. Tibshirani<sup>1,2</sup>  
ryantibs@stat.cmu.edu

<sup>1</sup> Machine Learning Department, Carnegie Mellon University, Pittsburgh, PA 15213

<sup>2</sup> Department of Statistics, Carnegie Mellon University, Pittsburgh, PA 15213

<sup>3</sup> Mathematics Department, University of California at San Diego, La Jolla, CA 10280

<sup>4</sup> Marianas Labs, Pittsburgh, PA 15213

## Abstract

We introduce a family of adaptive estimators on graphs, based on penalizing the  $\ell_1$  norm of discrete graph differences. This generalizes the idea of trend filtering [17, 38], used for univariate nonparametric regression, to graphs. Analogous to the univariate case, graph trend filtering exhibits a level of local adaptivity unmatched by the usual  $\ell_2$ -based graph smoothers. It is also defined by a convex minimization problem that is readily solved (e.g., by fast ADMM or Newton algorithms). We demonstrate the merits of graph trend filtering through both examples and theory.

**Keywords.** trend filtering, nonparametric regression, graph, local adaptivity

## 1 Introduction

Nonparametric regression has a rich history in statistics, carrying well over 50 years of associated literature. The goal of this paper is to port a successful idea in univariate nonparametric regression, trend filtering [34, 17, 38, 44], to the setting of estimation on graphs. The proposed estimator, graph trend filtering, shares three key properties of trend filtering in the univariate setting.

1. **Local adaptivity:** graph trend filtering can adapt to inhomogeneity in the level of smoothness of an observed signal across nodes. This stands in contrast to the usual  $\ell_2$ -based methods, e.g., Laplacian regularization [32], which enforce smoothness globally with a much heavier hand, and tends to yield estimates that are either smooth or else wiggly throughout.
2. **Computational efficiency:** graph trend filtering is defined by a regularized least squares problem, in which the penalty term is nonsmooth, but convex and structured enough to permit efficient large-scale computation.
3. **Analysis regularization:** the graph trend filtering problem directly penalizes (possibly higher order) differences in the fitted signal across nodes. Therefore graph trend filtering falls into what is called the *analysis* framework for defining estimators. Alternatively, in the *synthesis* framework, we would first construct a suitable basis over the graph, and then regress the observed signal over this basis; e.g., [30] study such an approach using wavelets; likewise, kernel methods regularize in terms of the eigenfunctions of the graph Laplacian [18]. An advantage of analysis regularization is that it easily yields complex extensions of the basic estimator by mixing penalties.

As a motivation example, consider a denoising problem on 402 census tracts of Allegheny County, PA, arranged into a graph with 402 vertices and 2382 edges obtained by connecting spatially adjacent tracts. To illustrate the adaptive property of graph trend filtering we generated an artificial signal with inhomogeneous smoothness across the nodes, and two sharp peaks near the center of the graph, as can be seen in the top left panel of Figure 1. (The signal was formed using a mixture of five Gaussians, in the underlying spatial coordinates.) We drew noisy observations around this signal, shown in the top right panel of the figure, and we fit graph trend filtering, graph Laplacian smoothing, and wavelet smoothing to these observations. Graph trend filtering is to be defined in Section 2 (here we used  $k = 2$ , quadratic order); the latter two, recall, are defined by the optimization problems

$$\min_{\beta \in \mathbb{R}^n} \|y - \beta\|_2^2 + \lambda \beta^\top L \beta \quad (\text{Laplacian smoothing}),$$

$$\min_{\theta \in \mathbb{R}^n} \frac{1}{2} \|y - W\theta\|_2^2 + \lambda \|\theta\|_1 \quad (\text{wavelet smoothing}).$$

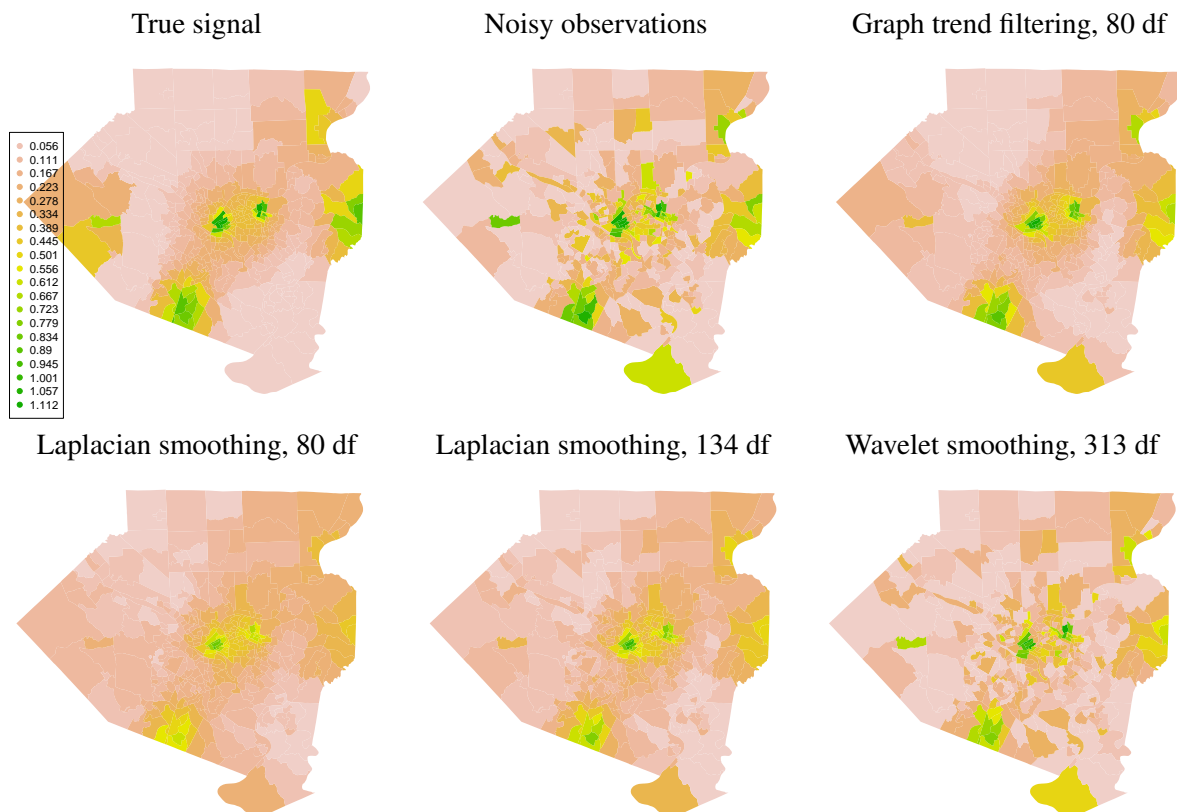


Figure 1: Color maps for the Allegheny County example.

Above,  $y \in \mathbb{R}^n$  is the vector of observations across nodes,  $n = 402$ ,  $L \in \mathbb{R}^{n \times n}$  is the unnormalized Laplacian matrix over the graph, and  $W \in \mathbb{R}^{n \times n}$  is a wavelet basis built over the graph (we followed the prescription of [30]). The three estimators each have their own regularization parameters  $\lambda$ ; since these are on different scales, we use effective degrees of freedom (df) as a common measure for the complexities of the fitted models.

The top right panel of Figure 1 shows the estimate from graph trend filtering with 80 df. We see that it adaptively fits to the sharp peaks in the center of the graph, and smooths out the surrounding regions appropriately. The graph Laplacian estimate with 80 df (bottom left), substantially oversmooths the high peaks in

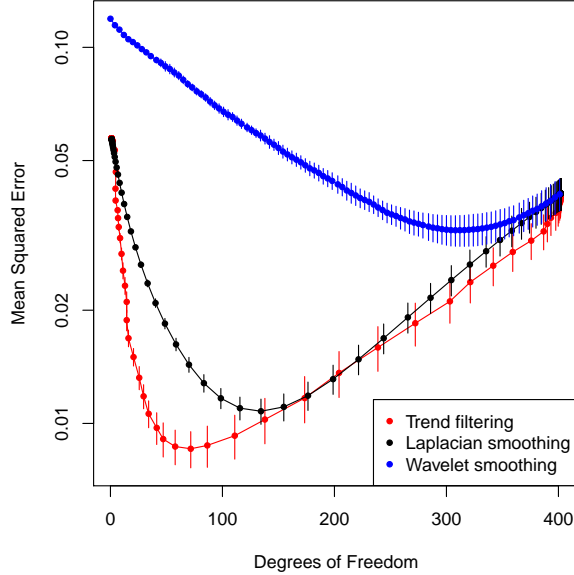


Figure 2: Mean squared errors for the Allegheny County example. Results were averaged over 10 simulations; the bars denote  $\pm 1$  standard errors.

the center, while at 134 df (bottom middle), it begins to detect the high peaks in the center, but undersmooths neighboring regions. Wavelet smoothing performs quite poorly across all df values—it appears to be most affected by the level of noise in the observations.

As a more quantitative assessment, Figure 2 shows the mean squared errors between the estimates and the true underlying signal. The differences in performance here are analogous to the univariate case, when comparing trend filtering to smoothing splines [38]. At smaller df values, Laplacian smoothing, due to its global considerations, fails to adapt to local differences across nodes. Trend filtering performs much better at low df values, and yet it matches Laplacian smoothing when both are sufficiently complex, i.e., in the overfitting regime. This demonstrates that the local flexibility of trend filtering estimates is a key attribute.

Here is an outline for the rest of this article. Section 2 defines graph trend filtering and gives underlying motivation and intuition. Section 3 covers basic properties and extensions of the graph trend filtering estimator. Section 4 examines computational approaches, and Section 5 looks at a number of both real and simulated data examples. Section 6 presents asymptotic error bounds for graph trend filtering. Section 7 concludes with a discussion. As for notation, we write  $X_A$  to extract the rows of a matrix  $X \in \mathbb{R}^{m \times n}$  that correspond to a subset  $A \subseteq \{1, \dots, m\}$ , and  $X_{-A}$  to extract the complementary rows. We use a similar convention for vectors:  $x_A$  and  $x_{-A}$  denote the components of a vector  $x \in \mathbb{R}^m$  that correspond to the set  $A$  and its complement, respectively. We write  $\text{row}(X)$  and  $\text{null}(X)$  for the row and null spaces of  $X$ , respectively, and  $X^\dagger$  for the pseudoinverse of  $X$ , with  $X^\dagger = (X^\top X)^\dagger X^\top$  when  $X$  is rectangular.

## 2 Trend Filtering on Graphs

### 2.1 Review: Univariate Trend Filtering

We begin by reviewing trend filtering in the univariate setting, where discrete difference operators play a central role. Suppose that we observe  $y = (y_1, \dots, y_n) \in \mathbb{R}^n$  across input locations  $x = (x_1, \dots, x_n) \in \mathbb{R}^n$ ; for simplicity, suppose that the inputs are evenly spaced, say,  $x = (1, \dots, n)$ . Given an integer  $k \geq 0$ , the

$k$ th order trend filtering estimate  $\hat{\beta} = (\hat{\beta}_1, \dots, \hat{\beta}_n)$  is defined as

$$\hat{\beta} = \underset{\beta \in \mathbb{R}^n}{\operatorname{argmin}} \frac{1}{2} \|y - \beta\|_2^2 + \lambda \|D^{(k+1)}\beta\|_1, \quad (1)$$

where  $\lambda \geq 0$  is a tuning parameter, and  $D^{(k+1)}$  is the discrete difference operator of order  $k + 1$ . When  $k = 0$ , problem (1) employs the first difference operator,

$$D^{(1)} = \begin{bmatrix} -1 & 1 & 0 & \dots & 0 \\ 0 & -1 & 1 & \dots & 0 \\ \vdots & & \ddots & \ddots & \\ 0 & 0 & \dots & -1 & 1 \end{bmatrix}. \quad (2)$$

Therefore  $\|D^{(1)}\beta\|_1 = \sum_{i=1}^{n-1} |\beta_{i+1} - \beta_i|$ , and the 0th order trend filtering estimate in (1) reduces to the 1-dimensional fused lasso estimator [37], also called 1-dimensional total variation denoising [26]. For  $k \geq 1$  the operator  $D^{(k+1)}$  is defined recursively by

$$D^{(k+1)} = D^{(1)}D^{(k)}, \quad (3)$$

with  $D^{(1)}$  above denoting the  $(n - k - 1) \times (n - k)$  version of the first difference operator in (2). In words,  $D^{(k+1)}$  is given by taking first differences of  $k$ th differences. The interpretation is hence that problem (1) penalizes the changes in the  $k$ th discrete differences of the fitted trend. The estimated components  $\hat{\beta}_1, \dots, \hat{\beta}_n$  exhibit the form of a  $k$ th order piecewise polynomial function, evaluated over the input locations  $x_1, \dots, x_n$ . This can be formally verified [38, 44] by examining a continuous-time analog of (1).

## 2.2 Trend Filtering over Graphs

Let  $G = (V, E)$  be an graph, with vertices  $V = \{1, \dots, n\}$  and undirected edges  $E = \{e_1, \dots, e_m\}$ , and suppose that we observe  $y = (y_1, \dots, y_n) \in \mathbb{R}^n$  over the nodes. Following the univariate definition in (1), we define the  $k$ th order *graph trend filtering* (GTF) estimate  $\hat{\beta} = (\hat{\beta}_1, \dots, \hat{\beta}_n)$  by

$$\hat{\beta} = \underset{\beta \in \mathbb{R}^n}{\operatorname{argmin}} \frac{1}{2} \|y - \beta\|_2^2 + \lambda \|\Delta^{(k+1)}\beta\|_1. \quad (4)$$

In broad terms, this problem (like univariate trend filtering) is a type of generalized lasso problem [39], in which the penalty matrix  $\Delta^{(k+1)}$  is a suitably defined *graph difference operator*, of order  $k + 1$ . In fact, the novelty in our proposal lies entirely within the definition of this operator.

When  $k = 0$ , we define first order graph difference operator  $\Delta^{(1)}$  in such a way it yields the graph-equivalent of a penalty on local differences:

$$\|\Delta^{(1)}\beta\|_1 = \sum_{(i,j) \in E} |\beta_i - \beta_j|.$$

so that the penalty term in (4) sums the absolute differences across connected nodes in  $G$ . To achieve this, we let  $\Delta^{(1)} \in \{-1, 0, 1\}^{m \times n}$  be the oriented incidence matrix of the graph  $G$ , containing one row for each edge in the graph; specifically, if  $e_\ell = (i, j)$ , then  $\Delta^{(1)}$  has  $\ell$ th row

$$\Delta_\ell^{(1)} = (0, \dots, \underset{\uparrow}{-1}_i, \dots, \underset{\uparrow}{1}_j, \dots, 0), \quad (5)$$

where the sign orientations are arbitrary. By construction, the 0th order graph trend filtering estimate is piecewise constant over nodes of  $G$ , and it coincides with the fused lasso (total variation regularized) estimate on the graph  $G$  [15, 39, 28].

For  $k \geq 1$ , we use a recursion to define the higher order graph difference operators, in a manner similar to the univariate case. The recursion alternates in multiplying by the first difference operator  $\Delta^{(1)}$  and its transpose (taking into account that this matrix not square:

$$\Delta^{(k+1)} = \begin{cases} (\Delta^{(1)})^\top \Delta^{(k)} = L^{\frac{k+1}{2}} & \text{for odd } k \\ \Delta^{(1)} \Delta^{(k)} = DL^{\frac{k}{2}} & \text{for even } k. \end{cases} \quad (6)$$

Above we exploited the fact that  $\Delta^{(2)} = (\Delta^{(1)})^\top \Delta^{(1)}$  is the unnormalized graph Laplacian  $L$  of  $G$ , and we abbreviated  $\Delta^{(1)}$  by  $D$ . Note that  $\Delta^{(k+1)} \in \mathbb{R}^{n \times n}$  for odd  $k$ , and  $\Delta^{(k+1)} \in \mathbb{R}^{m \times n}$  for even  $k$ .

An important point is that our defined graph difference operators (5), (6) reduce to the univariate ones (2), (3) in the case of a chain graph (in which  $V = \{1, \dots, n\}$  and  $E = \{(i, i+1) : i = 1, \dots, n-1\}$ ), modulo boundary terms. That is, when  $k$  is even, if one removes the first  $k/2$  rows and last  $k/2$  rows of  $\Delta^{(k+1)}$  for the chain graph, then one recovers  $D^{(k+1)}$ ; when  $k$  is odd, if one removes the first and last  $(k+1)/2$  rows of  $\Delta^{(k+1)}$  for the chain graph, then one recovers  $D^{(k+1)}$ . Further intuition for our graph difference operators is given next.

### 2.3 Piecewise Polynomials over Graphs

We give some insight for our definition of graph difference operators (5), (6), based on the idea of piecewise polynomials over graphs. In the univariate case, as described in Section 2.1, sparsity of  $\beta$  under the difference operator  $D^{(k+1)}$  implies a specific  $k$ th order piecewise polynomial structure for the components of  $\beta$  [38, 44]. Since the components of  $\beta$  correspond to (real-valued) input locations  $x = (x_1, \dots, x_n)$ , the interpretation of a piecewise polynomial here is unambiguous. But for a graph, one might ask: does sparsity of  $\Delta^{(k+1)}\beta$  mean that the components of  $\beta$  are piecewise polynomial? And what does the latter even mean, as the components of  $\beta$  are defined over the nodes? To address these questions, we intuitively *define* a piecewise polynomial over a graph, and show that it implies sparsity under our constructed graph difference operators.

- **Piecewise constant** ( $k = 0$ ): we say that a signal  $\beta$  is piecewise constant over a graph  $G$  if many of the differences  $\beta_i - \beta_j$  are zero across edges  $(i, j) \in E$  in  $G$ . Note that this is exactly the property associated with sparsity of  $\Delta^{(1)}\beta$ , since  $\Delta^{(1)} = D$ , the oriented incidence matrix of  $G$ .
- **Piecewise linear** ( $k = 1$ ): we say that a signal  $\beta$  has a piecewise linear structure over  $G$  if  $\beta$  satisfies

$$\beta_i - \frac{1}{n_i} \sum_{(i,j) \in E} \beta_j = 0,$$

for many nodes  $i \in V$ , where  $n_i$  is the number of nodes adjacent to  $i$ . In words, we are requiring that the signal components can be linearly interpolated from its neighboring values at many nodes in the graph. This is quite a natural notion of (piecewise) linearity: requiring that  $\beta_i$  be equal to the average of its neighboring values would enforce linearity at  $\beta_i$  under an appropriate embedding of the points in Euclidean space. Again, this is precisely the same as requiring  $\Delta^{(2)}\beta$  to be sparse, since  $\Delta^{(2)} = L$ , the graph Laplacian.

- **Piecewise polynomial** ( $k \geq 2$ ): We say that  $\beta$  has a piecewise quadratic structure over  $G$  if the first differences  $\alpha_i - \alpha_j$  of the second differences  $\alpha = \Delta^{(2)}\beta$  are mostly zero, over edges  $(i, j) \in E$ .

Likewise,  $\beta$  has a piecewise cubic structure over  $G$  if the second differences  $\alpha_i - \frac{1}{n_i} \sum_{(i,j) \in E} \alpha_j$  of the second differences  $\alpha = \Delta^{(2)}\beta$  are mostly zero, over nodes  $i \in V$ . This argument extends, alternating between leading first and second differences for even and odd  $k$ . Sparsity of  $\Delta^{(k+1)}\beta$  in either case exactly corresponds to many of these differences being zero, by construction.

In Figure 3, we illustrate the graph trend filtering estimator on a 2d grid graph of dimension  $20 \times 20$ , i.e., a grid graph with 400 nodes and 740 edges. For each of the cases  $k = 0, 1, 2$ , we generated synthetic measurements over the grid, and computed a GTF estimate of the corresponding order. We chose the 2d grid setting so that the piecewise polynomial nature of GTF estimates could be visualized. Below each plot, the utilized graph trend filtering penalty is displayed in more explicit detail.

## 2.4 $\ell_1$ versus $\ell_2$ Regularization

It is instructive to compare the graph trend filtering estimator, as defined in (4), (5), (6) to Laplacian smoothing [32]. Standard Laplacian smoothing uses the same least squares loss as in (4), but replaces the penalty term with  $\beta^\top L\beta$ . A natural generalization would be to allow for a power of the Laplacian matrix  $L$ , and define  $k$ th order graph Laplacian smoothing according to

$$\hat{\beta} = \underset{\beta \in \mathbb{R}^n}{\operatorname{argmin}} \|y - \beta\|_2^2 + \lambda \beta^\top L^{k+1} \beta. \quad (7)$$

The above penalty term can be written as  $\|L^{(k+1)/2}\beta\|_2^2$  for odd  $k$ , and  $\|DL^{k/2}\beta\|_2^2$  for even  $k$ ; i.e., this penalty is exactly  $\|\Delta^{(k+1)}\beta\|_2^2$  for the graph difference operator  $\Delta^{(k+1)}$  defined previously.

As we can see, the critical difference between graph Laplacian smoothing (7) and graph trend filtering (4) lies in the choice of penalty norm:  $\ell_2$  in the former, and  $\ell_1$  in the latter. The effect of the  $\ell_1$  penalty is that the GTF program can set many (higher order) graph differences to zero exactly, and leave others at large nonzero values; i.e., the GTF estimate can simultaneously be smooth in some parts of the graph and wiggly in others. On the other hand, due to the (squared)  $\ell_2$  penalty, the graph Laplacian smoother cannot set any graph differences to zero exactly, and roughly speaking, must choose between making all graph differences small or large. The relevant analogy here is the comparison between the lasso and ridge regression, or univariate trend filtering and smoothing splines [38], and the suggestion is that GTF can adapt to the proper local degree of smoothness, while Laplacian smoothing cannot. This is strongly supported by the examples given throughout this paper.

## 2.5 Related Work

Some authors from the signal processing community, e.g., [7, 27], have studied total generalized variation (TGV), a higher order variant of total variation regularization. Moreover, several discrete versions of these operators have been proposed. They are often similar to the construction that we have. However, the focus of this work is mostly on how well a discrete functional approximates its continuous counterpart. This is quite different from our concern, as a signal on a graph (say a social network) may not have any meaningful continuous-space embedding at all. In addition, we are not aware of any study on the statistical properties of these regularizers. In fact, our theoretical analysis in Section 6 may be extended to these methods too.

# 3 Properties and Extensions

## 3.1 Basic Structure and Degrees of Freedom

We now describe the basic structure of graph trend filtering estimates and present an unbiased estimate for their degrees of freedom. Let the tuning parameter  $\lambda$  be arbitrary but fixed. By virtue of the  $\ell_1$  penalty in (4),

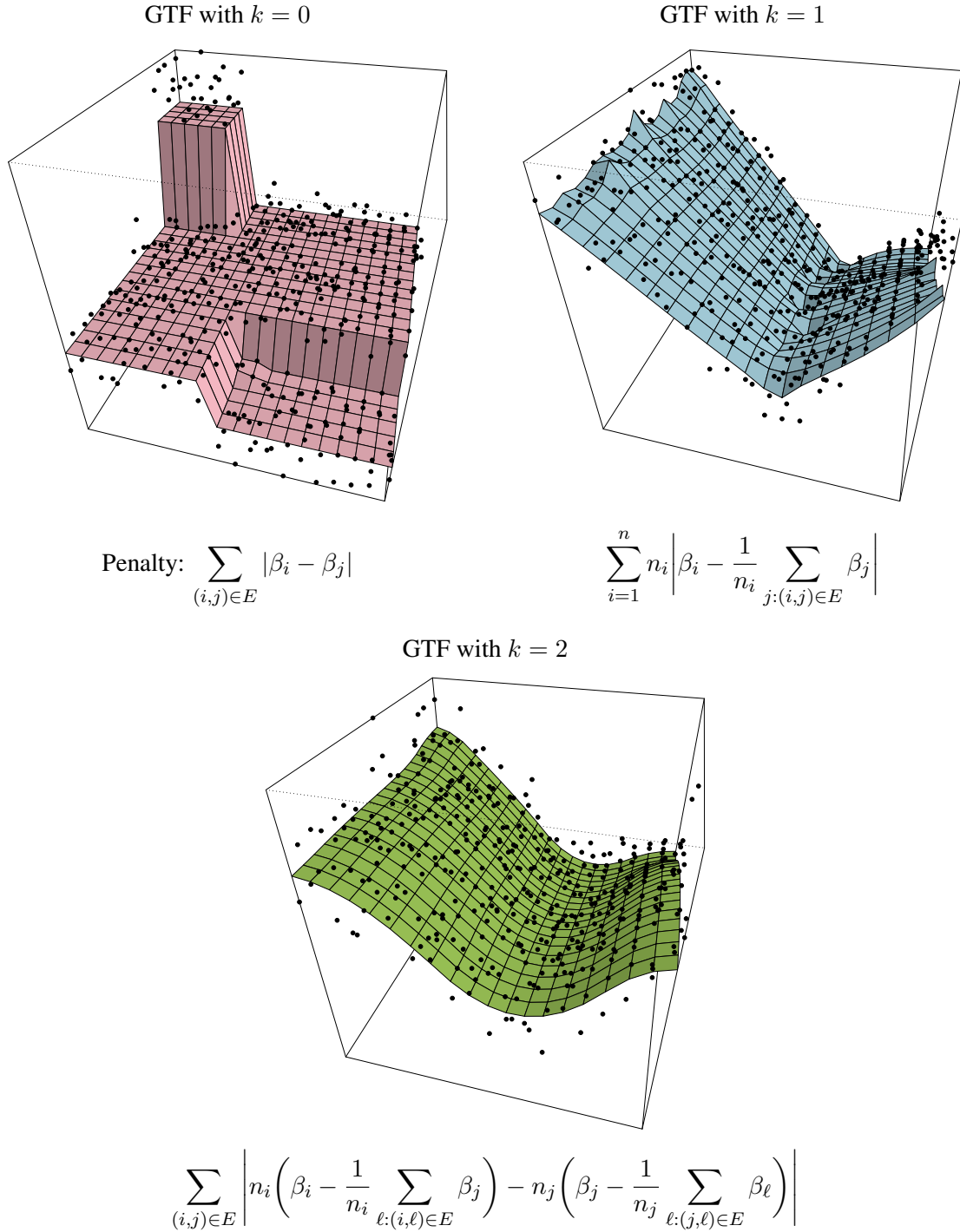


Figure 3: Graph trend filtering estimates of orders  $k = 0, 1, 2$  on a 2d grid. The utilized  $\ell_1$  graph difference penalties are shown in elementwise detail below each plot (first, second, and third order graph differences).

the solution  $\hat{\beta}$  satisfies  $\text{supp}(\Delta^{(k+1)}\hat{\beta}) = A$  for some active set  $A$  (typically  $A$  is smaller when  $\lambda$  is larger). Trivially, we can reexpress this as  $\Delta_{-A}^{(k+1)}\hat{\beta} = 0$ , or  $\hat{\beta} \in \text{null}(\Delta_{-A}^{(k+1)})$ . Therefore, the basic structure of GTF estimates is revealed by analyzing the null space of the suboperator  $\Delta_{-A}^{(k+1)}$ .

**Lemma 1.** *Assume without a loss of generality that  $G$  is connected (otherwise the results apply to each connected component of  $G$ ). Let  $D, L$  be the oriented incidence matrix and Laplacian matrix of  $G$ .*

*For even  $k$ , let  $A \subseteq \{1, \dots, m\}$ , and let  $G_{-A}$  denote the subgraph induced by removing the edges indexed by  $A$  (i.e., removing edges  $e_\ell$ ,  $\ell \in A$ ). Let  $C_1, \dots, C_s$  be the connected components of  $G_{-A}$ . Then*

$$\text{null}(\Delta_{-A}^{(k+1)}) = \text{span}\{\mathbf{1}\} + (L^\dagger)^{\frac{k}{2}} \text{span}\{\mathbf{1}_{C_1}, \dots, \mathbf{1}_{C_s}\},$$

*where  $\mathbf{1} = (1, \dots, 1) \in \mathbb{R}^n$ , and  $\mathbf{1}_{C_1}, \dots, \mathbf{1}_{C_s} \in \mathbb{R}^n$  are the indicator vectors over connected components. For odd  $k$ , let  $A \subseteq \{1, \dots, n\}$ . Then*

$$\text{null}(\Delta_{-A}^{(k+1)}) = \text{span}\{\mathbf{1}\} + \{(L^\dagger)^{\frac{k+1}{2}} v : v_{-A} = 0\}.$$

The proof of Lemma 1 is straightforward and so we omit it. The lemma is useful for a few reasons. First, as motivated above, it describes the coarse structure of GTF solutions. When  $k = 0$ , we can see (as  $(L^\dagger)^{k/2} = I$ ) that  $\hat{\beta}$  will indeed be piecewise constant over groups of nodes  $C_1, \dots, C_s$  of  $G$ . For  $k = 2, 4, \dots$ , this structure is smoothed by multiplying such piecewise constant levels by  $(L^\dagger)^{k/2}$ . Meanwhile, for  $k = 1, 3, \dots$ , the structure of the GTF estimate is based on assigning nonzero values to a subset  $A$  of nodes, and then smoothing through multiplication by  $(L^\dagger)^{(k+1)/2}$ . Both of these smoothing operations, which depend on  $L^\dagger$ , have interesting interpretations in terms of to the electrical network perspective for graphs. This is given in the next subsection.

A second use of Lemma 1 is that it leads to a simple expression for the degrees of freedom, i.e., the effective number of parameters, of the GTF estimate  $\hat{\beta}$ . From results on generalized lasso problems [39, 40], we have  $\text{df}(\hat{\beta}) = \mathbb{E}[\text{nullity}(\Delta_{-A}^{(k+1)})]$ , with  $A$  denoting the support of  $\Delta^{(k+1)}\hat{\beta}$ , and  $\text{nullity}(X)$  the dimension of the null space of a matrix  $X$ . Applying Lemma 1 then gives the following.

**Lemma 2.** *Assume that  $G$  is connected. Let  $\hat{\beta}$  denote the GTF estimate at a fixed but arbitrary value of  $\lambda$ . Under the normal error model  $y \sim \mathcal{N}(\beta_0, \sigma^2 I)$ , the GTF estimate  $\hat{\beta}$  has degrees of freedom*

$$\text{df}(\hat{\beta}) = \begin{cases} \mathbb{E}[\max\{|A|, 1\}] & \text{odd } k, \\ \mathbb{E}[\text{number of connected components of } G_{-A}] & \text{even } k. \end{cases}$$

*Here  $A = \text{supp}(\Delta^{(k+1)}\hat{\beta})$  denotes the active set of  $\hat{\beta}$ .*

As a result of Lemma 2, we can form simple unbiased estimate for  $\text{df}(\hat{\beta})$ ; for  $k$  odd, this is  $\max\{|A|, 1\}$ , and for  $k$  even, this is the number of connected components of  $G_{-A}$ , where  $A$  is the support of  $\Delta^{(k+1)}\hat{\beta}$ . When reporting degrees of freedom for graph trend filtering (as in the example in the introduction), we use these unbiased estimates.

### 3.2 Electrical Network Interpretation

Lemma 1 reveals a mathematical structure for GTF estimates  $\hat{\beta}$ , which satisfy  $\hat{\beta} \in \Delta_{-A}^{(k+1)}$  for some set  $A$ . It is interesting to interpret the results using the electrical network perspective for graphs [43]. In this perspective, we think of replacing each edge in the graph with a resistor of value 1. If  $c \in \mathbb{R}^n$  is a vector that describes how much current is going in at each node in the graph, then  $v = Lc$  describes the induced voltage at each node. Provided that  $\mathbf{1}^\top c = 0$ , which means that the total accumulation of current in the network is 0, we can solve for the current values from the voltage values:  $c = L^\dagger v$ .



The odd case in Lemma 1 asserts that

$$\text{null}(\Delta_{-A}^{(k+1)}) = \text{span}\{\mathbf{1}\} + \{(L^\dagger)^{\frac{k+1}{2}} v : v_{-A} = 0\}.$$

For  $k = 1$ , this says that GTF estimates are formed by assigning a sparse number of nodes in the graph a nonzero voltage  $v$ , then solving for the induced current  $L^\dagger v$  (and shifting this entire current vector by a constant amount). For  $k = 3$ , we assign a sparse number of nodes a nonzero voltage, solve for the induced current, and then *repeat this*: we relabel the induced current as input voltages to the nodes, and compute the new induced current. This process is again iterated for  $k = 5, 7, \dots$

The even case in Lemma 1 asserts that

$$\text{null}(\Delta_{-A}^{(k+1)}) = \text{span}\{\mathbf{1}\} + (L^\dagger)^{\frac{k}{2}} \text{span}\{\mathbf{1}_{C_1}, \dots, \mathbf{1}_{C_s}\}.$$

For  $k = 2$ , this result says that GTF estimates are given by choosing a partition  $C_1, \dots, C_s$  of the nodes, and assigning a constant input voltage to each element of the partition. We then solve for the induced current (and potentially shift this by an overall constant amount). The process is iterated for  $k = 4, 6, \dots$  by relabeling the induced current as input voltage.

The comparison between the structure of estimates for  $k = 2$  and  $k = 3$  is informative: in a sense, the above tells us that 2nd order GTF estimates will be *smoother* than 3rd order estimates, as a sparse input voltage vector need not induce a current that is piecewise constant over nodes in the graph. For example, an input voltage vector that has only a few nodes with very large nonzero values will induce a current that is peaked around these nodes, but not piecewise constant.

### 3.3 Extensions

Several extensions of the proposed graph trend filtering model are possible. Trend filtering over a weighted graph, for example, could be performed by using a properly weighted version of the edge incidence matrix in (5), and carrying forward the same recursion in (6) for the higher order difference operators. As another example, the Gaussian regression loss in (4) could be changed to another suitable likelihood-derived losses in order to accommodate a different data type for  $y$ , say, logistic regression loss for binary data, or Poisson regression loss for count data.

In Section 5.2, we explore a modest extension of GTF, where we add a strongly convex prior term to the criterion in (4) to assist in performing graph-based imputation from partially observed data over the nodes. In Section 5.3, we investigate a modification of the proposed regularization scheme, where we add a pure  $\ell_1$  penalty on  $\beta$  in (4), hence forming a sparse variant of GTF. Other potentially interesting penalty extensions include: mixing graph difference penalties of various orders, and tying together several denoising tasks with a group penalty. Extensions such as these are easily built, recall, as a result of the analysis framework used by the GTF program, wherein the estimate defined through direct regularization via an analyzing operator, the  $\ell_1$ -based graph difference penalty  $\|\Delta^{(k+1)}\beta\|_1$ .

## 4 Computation

Graph trend filtering is defined by a convex optimization problem (4). In principle this means that (at least for small or moderately sized problems) its solutions can be reliably computed using a variety of standard algorithms. In order to handle large-scale problems, we describe two specialized algorithms that improve on generic procedures by taking advantage of the structure of  $\Delta^{(k+1)}$ .

## 4.1 A Fast ADMM Algorithm

We reparametrize (4) by introducing auxiliary variables, so that we can apply ADMM. For even  $k$ , we use a special transformation that is critical for fast computation (following [25] in univariate trend filtering); for odd  $k$ , this is not possible. The reparametrizations for even and odd  $k$  are

$$\begin{aligned} \min_{\beta, z \in \mathbb{R}^n} \frac{1}{2} \|y - \beta\|_2^2 + \lambda \|Dz\|_1 \quad \text{s.t.} \quad z = L^{\frac{k}{2}} x, \\ \min_{\beta, z \in \mathbb{R}^n} \frac{1}{2} \|y - \beta\|_2^2 + \lambda \|z\|_1 \quad \text{s.t.} \quad z = L^{\frac{k+1}{2}} x, \end{aligned}$$

respectively. Recall that  $D$  is the oriented incidence matrix and  $L$  is the graph Laplacian. The augmented Lagrangian is

$$\frac{1}{2} \|y - \beta\|_2^2 + \lambda \|Sx\|_1 + \frac{\rho}{2} \|z - L^q \beta + u\|_2^2 - \frac{\rho}{2} \|u\|_2^2,$$

where  $S = D$  or  $S = I$  depending on whether  $k$  is even or odd, and likewise  $q = k/2$  or  $q = (k+1)/2$ . ADMM then proceeds by iteratively minimizing the augmented Lagrangian over  $\beta$ , minimizing over  $z$ , and performing a dual update over  $u$ . The  $\beta$  and  $z$  updates are of the form

$$\beta \leftarrow (I + \rho L^{2q})^{-1} b, \tag{8}$$

$$z \leftarrow \operatorname{argmin}_{x \in \mathbb{R}^n} \frac{1}{2} \|b - x\|_2^2 + \frac{\lambda}{\rho} \|Sx\|_1, \tag{9}$$

for some  $b$ . The linear system in (8) is well-conditioned, sparse, and can be solved efficiently using the preconditioned conjugate gradient method. This involves only multiplication with Laplacian matrices. For a small enough  $\rho$  (augmented Lagrangian parameter), the system (8) is diagonally dominant, and thus we can solve it in almost linear time using special Laplacian/SDD solvers [33, 19, 16].

The update in (9) is simply given by soft-thresholding when  $S = I$ , and when  $S = D$  it is given by graph TV denoising, i.e., given solving by solving a graph fused lasso problem. Note that this subproblem has the exact structure of the graph trend filtering problem (4) with  $k = 0$ . A direct approach for graph TV denoising is available based on parametric max-flow [10], and this algorithm is empirically much faster than its worst-case complexity [6]. In the special case that the underlying graph is a grid, a promising alternative method employs proximal stacking techniques [3].

## 4.2 A Fast Newton Method

As an alternative to ADMM, a projected Newton-type method [4, 2] can be used to solve (4) via its dual problem:

$$\hat{v} = \operatorname{argmin}_{v \in \mathbb{R}^T} \|y - (\Delta^{(k+1)})^\top v\|_2^2 \quad \text{s.t.} \quad \|v\|_\infty \leq \lambda.$$

The solution of (4) is then given by  $\hat{\beta} = y - (\Delta^{(k+1)})^\top \hat{v}$ . (For univariate trend filtering, [17] adopt a similar strategy, but instead use an interior point method.) The projected Newton method performs updates using a reduced Hessian, so abbreviating  $\Delta = \Delta^{(k+1)}$ , each iteration boils down to

$$v \leftarrow a + (\Delta_I^\top)^\dagger b, \tag{10}$$

for some  $a, b$  and set of indices  $I$ . The linear system in (10) is always sparse, but conditioning becomes an issue as  $k$  grows (note: the same problem does not exist in (8) because of the padding by the identity matrix  $I$ ). We have found empirically that a preconditioned conjugate gradient method works quite well for (10) for  $k = 1$ , but for larger  $k$  it can struggle due to poor conditioning.

### 4.3 Computation Summary

In our experience with practical experiments, the following algorithms work best for the various graph trend orders  $k$ .

Order	Algorithm
$k = 0$	Parametric max-flow
$k = 1$	Projected Newton method
$k = 2, 4, \dots$	ADMM with parametric max-flow
$k = 3, 5, \dots$	ADMM with soft-thresholding

Figure 4 compares performances of the various algorithms on a moderately large simulated example, using a 2d grid graph. We can see that the projected Newton method converges faster than ADMM (superlinear versus at best linear convergence), so when its updates can be performed efficiently ( $k = 1$ ), it is preferred. The figure also shows that the special ADMM algorithm (with max-flow) converges faster than the naive one (with soft-thresholding), so when applicable ( $k = 2$ ), it is preferred. We remark that orders the  $k = 0, 1, 2$  are of most practical interest, so we do not often run naive ADMM with soft-thresholding.

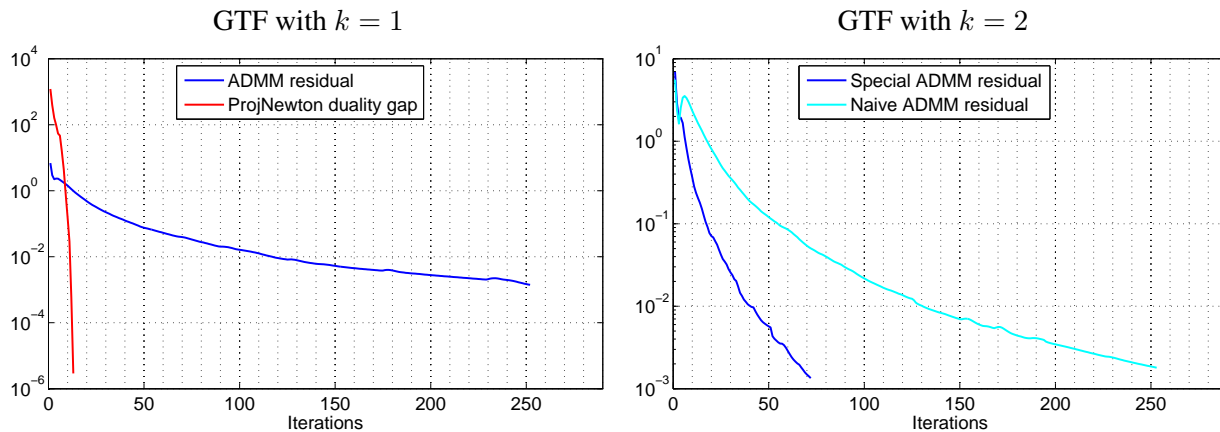


Figure 4: Convergence plots for projected Newton method and ADMM for solving GTF with  $k = 1$  and  $k = 2$ . The algorithms are all run on a 2d grid graph (an image) with 16,384 nodes and 32,512 edges. For projected Newton, we plot the duality gap across iterations; for the ADMM routines, we plot the average of the primal and dual residuals in the ADMM framework (which also serves as a valid suboptimality bound).

## 5 Examples

### 5.1 Trend Filtering over the Facebook Graph

In the Introduction, we examined the denoising power of graph trend filtering in a spatial setting. Here we examine the behavior of graph trend filtering on a nonplanar graph: the Facebook graph from the Stanford Network Analysis Project (<http://snap.stanford.edu>). This is composed of 4039 nodes representing Facebook users, and 88,234 edges representing friendships, collected from real survey participants; the graph has one connected component, but the observed degree sequence is very mixed, ranging from 1 to 1045 (see [24] for more details).

We generated synthetic measurements over the Facebook nodes (users) based on three different ground truth models, so that we can precisely evaluate and compare the estimation accuracy of GTF, Laplacian

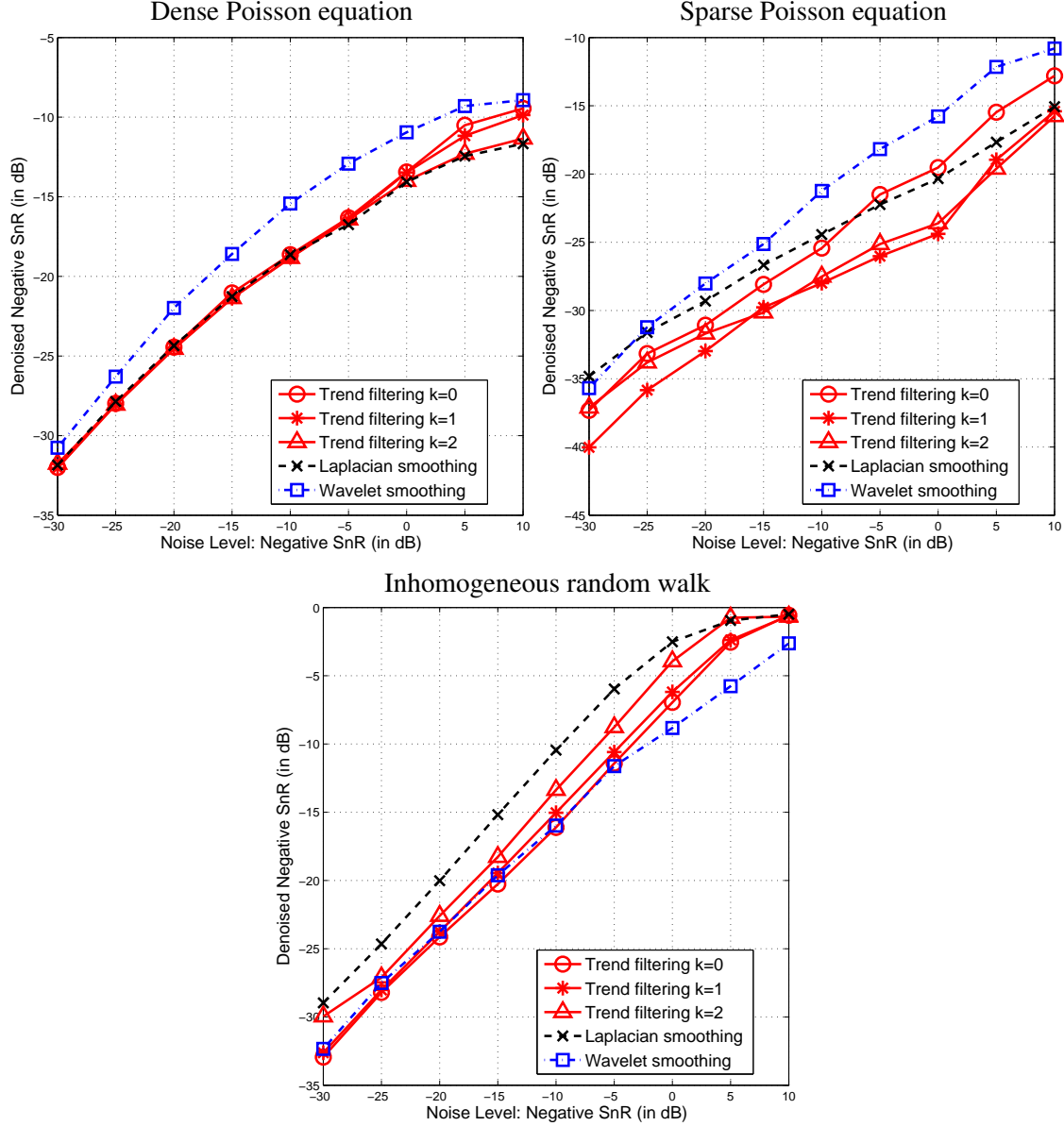


Figure 5: Performance of GTF and others for three generative models on the Facebook graph. The x-axis shows the negative SnR:  $10 \log_{10}(n\sigma^2/\|x\|_2^2)$ , where  $n = 4039$ ,  $x$  is the underlying signal, and  $\sigma^2$  is the noise variance. Hence the noise level is increasing from left to right. The y-axis shows the denoised negative SnR:  $10 \log_{10}(\text{MSE}/\|x\|_2^2)$ , where MSE denotes mean squared error, so the achieved MSE is increasing from bottom to top.

smoothing, and wavelet smoothing. The three ground truth models represent very different scenarios for the underlying signal  $x$ , each one favorable to different estimation methods. These are:

1. **Dense Poisson equation:** we solved the Poisson equation  $Lx = b$  for  $x$ , where  $b$  is arbitrary and dense (its entries were i.i.d. normal draws).
2. **Sparse Poisson equation:** we solved the Poisson equation  $Lx = b$  for  $x$ , where  $b$  is sparse and has 30 nonzero entries (again i.i.d. normal draws).

3. **Inhomogeneous random walk:** we ran a set of decaying random walks at different starter nodes in the graph, and recorded in  $x$  the total number of visits at each node. Specifically, we chose 10 nodes as starter nodes, and assigned each starter node a decay probability uniformly at random between 0 and 1 (this is the probability that the walk terminates at each step instead of travelling to a neighboring node). At each starter node, we also sent out a varying number of random walks, chosen uniformly between 0 and 1000.

In each case, the synthetic measurements were formed by adding noise to  $x$ . We note that model 1 is designed to be favorable for Laplace smoothing; model 2 is designed to be favorable for GTF; and in the inhomogeneity in model 3 is designed to be challenging for Laplacian smoothing, and favorable for the more adaptive GTF and wavelet methods.

Figure 5 shows the performance of the three estimation methods, over a wide range of noise levels in the synthetic measurements; performance here is measured by the best achieved mean squared error, allowing each method to be tuned optimally at each noise level. The summary: GTF estimates are (expectedly) superior when the Laplacian-based sparsity pattern is in effect (model 2), but are nonetheless highly competitive in both other settings—the dense case, in which Laplacian smoothing thrives, and the inhomogeneous random walk case, in which wavelets thrive.

## 5.2 Graph-Based Transductive Learning over UCI Data

Graph trend filtering can be used for graph-based transductive learning, as motivated by the work of [35, 36], who rely on Laplacian regularization. Consider a semi-supervised learning setting, where we are given only a small number of seed labels over nodes of a graph, and the goal is to impute the labels on the remaining nodes. Write  $O \subseteq \{1, \dots, n\}$  for the set of observed nodes, and assume that each observed label falls into  $\{1, \dots, K\}$ . Then we can define the modified absorption problem under graph trend filtering regularization (MAD-GTF) by

$$\hat{B} = \operatorname{argmin}_{B \in \mathbb{R}^{n \times K}} \sum_{j=1}^K \sum_{i \in O} (Y_{ij} - B_{ij})^2 + \lambda \sum_{j=1}^K \|\Delta^{(k+1)} B_j\|_1 + \epsilon \sum_{j=1}^K \|R_j - B_j\|_2^2. \quad (11)$$

The matrix  $Y \in \mathbb{R}^{n \times K}$  is an indicator matrix: each observed row  $i \in O$  is described by  $Y_{ij} = 1$  if class  $j$  is observed and  $Y_{ij} = 0$  otherwise. The matrix  $B \in \mathbb{R}^{n \times K}$  contains fitted probabilities, with  $B_{ij}$  giving the probability that node  $i$  is of class  $j$ . We write  $B_j$  for its  $j$ th column, and hence the middle term in the above criterion encourages each set of class probabilities to behave smoothly over the graph. The last term in the above criterion ties the fitted probabilities to some given prior weights  $R \in \mathbb{R}^{n \times K}$ . In principle  $\epsilon$  could act as a second tuning parameter, but for simplicity we take  $\epsilon$  to be small and fixed, with any  $\epsilon > 0$  guaranteeing that the criterion in (11) is strictly convex, and thus has a unique solution  $\hat{B}$ . The entries of  $\hat{B}$  need not be probabilities in any strict sense, but we can still interpret them as relative probabilities, and imputation can be performed by assigning each unobserved node  $i \notin O$  a class label  $j$  such that  $\hat{B}_{ij}$  is largest.

Our specification of MAD-GTF only deviates from the MAD proposal of [35] in that these authors used the Laplacian regularization term  $\sum_{j=1}^K B_j^\top L B_j$ , in place of  $\ell_1$ -based graph difference regularizer in (11). If the underlying class probabilities are thought to have heterogeneous smoothness over the graph, then replacing the Laplacian regularizer with the GTF-designed one might lead to better performance. As a broad comparison of the two methods, we ran them on the 11 most popular classification data sets from the UCI Machine Learning repository (<http://archive.ics.uci.edu/ml/>).<sup>1</sup> For each data set, we constructed a 5-nearest-neighbor graph based on the Euclidean distance between provided features, and

<sup>1</sup>We used all data sets here, except the “forest-fires” data set, which is a regression problem. Also, we zero-filled the missing data in “internet-ads” data set and used a random one third of the data in the “poker” data set.

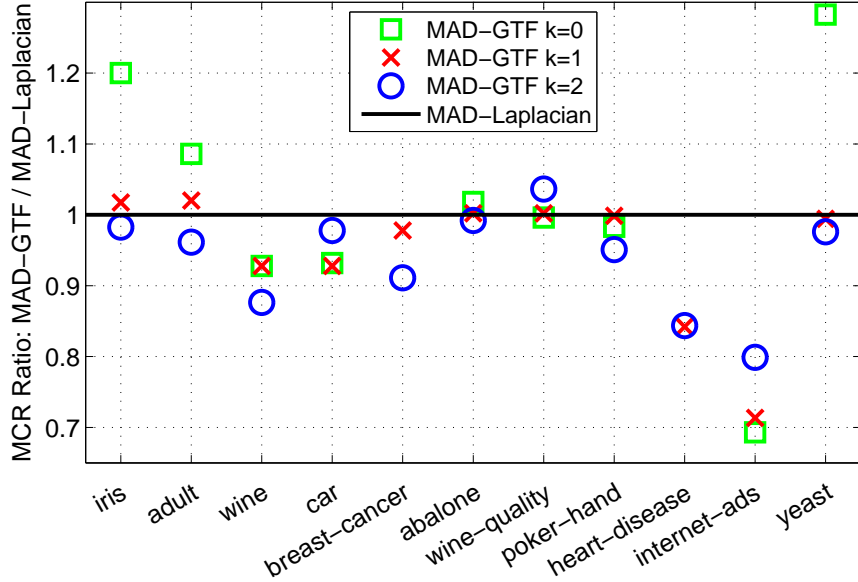


Figure 6: Ratio of the misclassification rate of MAD-GTF to MAD-Laplacian, for graph-based imputation, on the 11 most popular UCI classification data sets.

# of classes	iris 3	adult 2	wine 3	car 4	breast-can. 2	abalone 29	wine-qual. 6	poker 10	heart-dis. 2	ads 2	yeast 10
Laplacian	0.085	0.270	0.060	0.316	0.064	0.872	0.712	0.814	0.208	0.306	0.566
GTF $k = 0$	0.102	0.293	0.055	<i>0.294</i>	<i>0.500</i>	<i>0.888</i>	0.709	0.801	<i>0.472</i>	<b>0.212</b>	0.726
p-value	0.254	0.648	0.406	<i>0.091</i>	<i>0.000</i>	<i>0.090</i>	0.953	0.732	<i>0.000</i>	<b>0.006</b>	<i>0.000</i>
GTF $k = 1$	0.087	0.275	<b>0.055</b>	<b>0.293</b>	0.063	0.874	0.713	0.813	0.175	<b>0.218</b>	0.563
p-value	0.443	0.413	<b>0.025</b>	<b>0.012</b>	0.498	0.699	0.920	0.801	0.134	<b>0.054</b>	0.636
GTF $k = 2$	0.084	0.259	<b>0.052</b>	0.309	<b>0.059</b>	0.865	0.738	0.774	0.175	0.244	<b>0.552</b>
p-value	0.798	0.482	<b>0.024</b>	0.523	<b>0.073</b>	0.144	0.479	0.138	0.301	0.212	<b>0.100</b>

Table 1: Misclassification rates of MAD-Laplacian and MAD-GTF for imputation in the UCI data sets. We also compute p-values over the 10 repetitions for each data set (10 draws of nodes to serve as seed labels) via paired t-tests. Cases where MAD-GTF achieves significantly better misclassification rate, at the 0.1 level, are highlighted in bold; cases where MAD-GTF achieves a significantly worse misclassification rate, at the 0.1 level, are highlighted in italics.

randomly selected 5 seeds per class to serve as the observed class labels. Then we set  $\epsilon = 0.01$ , used prior weights  $R_{ij} = 1/K$  for all  $i$  and  $j$ , and chose the tuning parameter  $\lambda$  over a wide grid of values to represent the best achievable performance by each method, on each experiment. Figure 6 and Table 1 summarize the misclassification rates from imputation using MAD-Laplacian and MAD-GTF, averaged over 10 repetitions of the randomly selected seed labels. We see that MAD-GTF with  $k = 0$  (basically a graph partition akin to MRF-based graph cut, using an Ising model) does not seem to work as well as the smoother alternatives. But MAD-GTF with  $k = 1$  and  $k = 2$  performs at least as well (and sometimes better) than MAD-Laplacian on each one of the UCI data sets. Recall that these data sets were selected entirely based on their popularity, and not at all on the belief that they might represent favorable scenarios for GTF (i.e., not on the prospect that they might exhibit some heterogeneity in the distribution of class labels over their respective graphs). Therefore, the fact that MAD-GTF nonetheless performs competitively in such a broad range of experiments is convincing evidence for the utility of the GTF regularizer.

### 5.3 Event Detection with NYC Taxi Trips Data

We illustrate a sparse variant of our proposed regularizers, given by adding a pure  $\ell_1$  penalty to the coefficients in (4), as in

$$\hat{\beta} = \operatorname{argmin}_{\beta \in \mathbb{R}^n} \frac{1}{2} \|y - \beta\|_2^2 + \lambda_1 \|\Delta^{(k+1)}\beta\|_1 + \lambda_2 \|\beta\|_1. \quad (12)$$

We call this *sparse graph trend filtering*, now with two tuning parameters  $\lambda_1, \lambda_2 \geq 0$ . Under the proper tuning, the sparse GTF estimate will be zero at many nodes in the graph, and will otherwise deviate smoothly from zero. This can be useful in situations where the observed signal represents a difference between two smooth processes that are mostly similar, but exhibit (perhaps significant) differences over a few regions of the graph. Here we apply it to the problem of detecting events based on abnormalities in the number of taxi trips at different locations of New York city. This data set was kindly provided by authors of [12], who obtained the data from NYC Taxi & Limosine Commission.<sup>2</sup> Specifically, we consider the graph to be the road network of Manhattan, which contains 3874 nodes (junctions) and 7070 edges (sections of roads that connect two junctions). For measurements over the nodes, we used the number of taxi pickups and dropoffs over a particular time period of interest: 12:00–2:00 pm on June 26, 2011, corresponding to the Gay Pride parade. As pickups and dropoffs do not generically occur at road junctions, we used interpolation to form counts over the graph nodes. A baseline seasonal average was calculated by considering data from the same time block 12:00–2:00 pm on the same day of the week across the nearest eight weeks. Thus the measurements  $y$  were then taken to be the difference between the counts observed during the Gay Pride parade and the seasonal averages.

Note that the nonzero node estimates from sparse GTF applied to  $y$ , after proper tuning, mark events of interest, because they convey substantial differences between the observed and expected taxi counts. According to descriptions in the news, we know that the Gay Pride parade was a giant march down at noon from 36th St. and Fifth Ave. all the way to Christopher St. in Greenwich Village, and traffic was blocked over the entire route for two hours (meaning no pickups and dropoffs could occur). We therefore hand-labeled this route as a crude “ground truth” for the event of interest, illustrated in the left panel of Figure 7.

In the bottom two panels of Figure 7, we compare sparse GTF (with  $k = 0$ ) and a sparse variant of Laplacian smoothing, obtained by replacing the first regularization term in (12) by  $\beta^\top L\beta$ . For a qualitative visual comparison, the smoothing parameter  $\lambda_1$  was chosen so that both methods have 200 degrees of freedom (without any sparsity imposed). The sparsity parameter was then set as  $\lambda_2 = 0.2$ . Similar to what we have seen already, GTF is able to better localize its estimates around strong inhomogenous spikes in the measurements, and is able to better capture the event of interest. The result of sparse Laplacian smoothing is far from localized around the ground truth event, and displays many nonzero node estimates throughout distant regions of the graph. If we were to decrease its flexibility (increase the smoothing parameter  $\lambda_1$  in its problem formulation), then the sparse Laplacian output would display more smoothness over the graph, but the node estimates around the ground truth region would also be grossly shrunken.

## 6 Estimation Error Bounds

In this section, we assume that  $y \sim \mathcal{N}(\beta_0, \sigma^2 I)$ , and study asymptotic error rates for graph trend filtering. (The assumption of a normal error model could be relaxed, but is used for simplicity). Our analysis actually focuses more broadly on the generalized lasso problem

$$\hat{\beta} = \operatorname{argmin}_{\beta \in \mathbb{R}^n} \frac{1}{2} \|y - \beta\|_2^2 + \lambda \|\Delta\beta\|_1, \quad (13)$$

<sup>2</sup>These authors also considered event detection, but their topological definition of an “event” is very different from what we considered here, and hence our results not directly comparable.

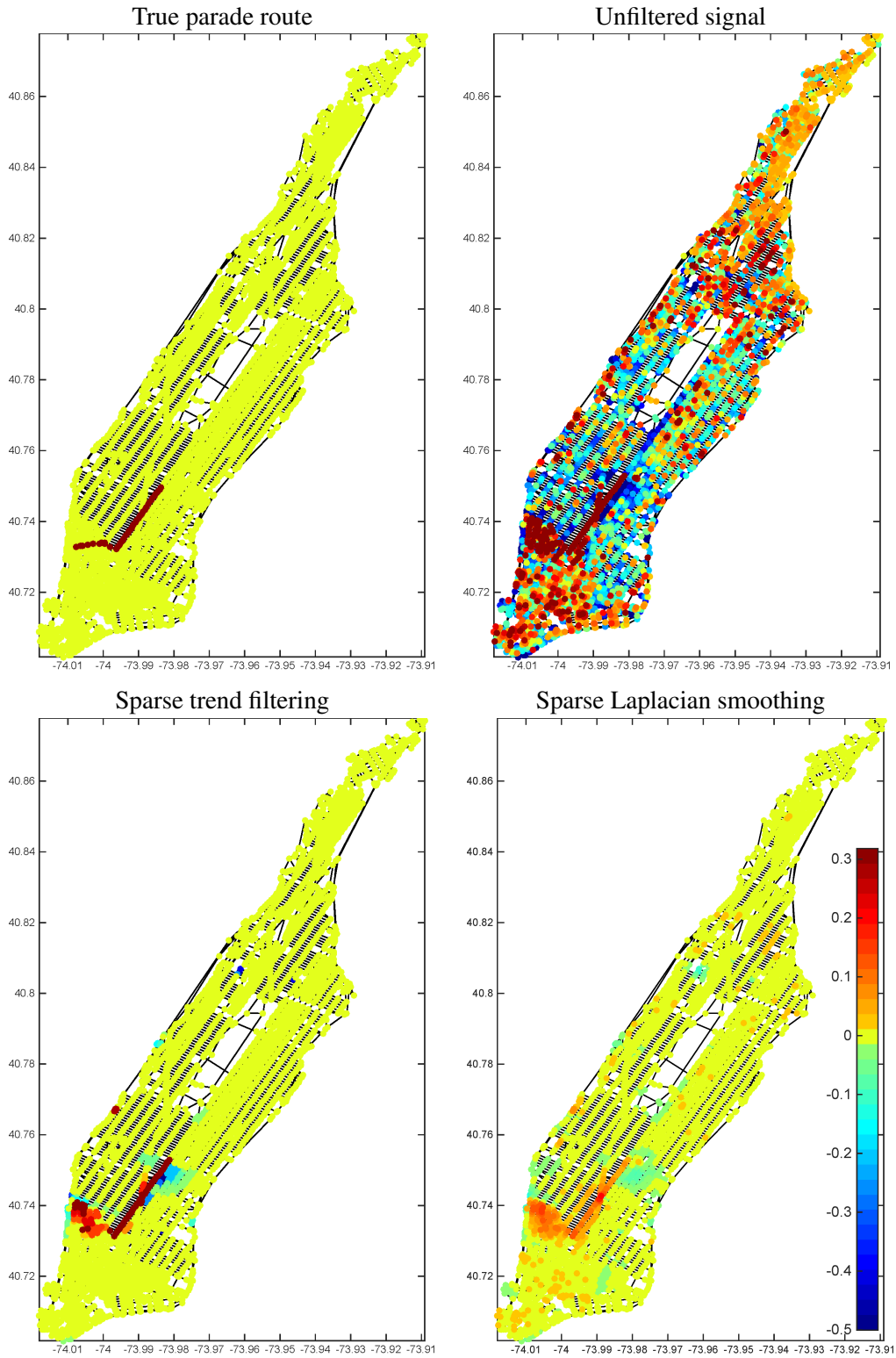


Figure 7: Comparison of sparse GTF and sparse Laplacian smoothing. We can see qualitatively that sparse GTF delivers better event detection with fewer false positives (zoomed-in, the sparse Laplacian plot shows a scattering of many non-zero colors).



where  $\Delta \in \mathbb{R}^{r \times n}$  is an arbitrary linear operator, and  $r$  denotes its number of rows. Throughout, we specialize the derived results to the graph difference operator  $\Delta = \Delta^{(k+1)}$ , to obtain concrete statements about GTF over particular graphs. All proofs are deferred to the Appendix.

## 6.1 Basic Error Bounds

Using similar arguments to the basic inequality for the lasso [8], we have the following preliminary bound.

**Theorem 3.** *Let  $M$  denote the maximum  $\ell_2$  norm of the columns of  $\Delta^\dagger$ . Then for a tuning parameter value  $\lambda = \Theta(M\sqrt{\log r})$ , the generalized lasso estimate  $\hat{\beta}$  in (13) has average squared error*

$$\frac{\|\hat{\beta} - \beta_0\|_2^2}{n} = O_{\mathbb{P}} \left( \frac{\text{nullity}(\Delta)}{n} + \frac{M\sqrt{\log r}}{n} \cdot \|\Delta\beta_0\|_1 \right).$$

Recall that  $\text{nullity}(\Delta)$  denotes the dimension of the null space of  $\Delta$ . For the GTF operator  $\Delta^{(k+1)}$  of any order  $k$ , note that  $\text{nullity}(\Delta^{(k+1)})$  is the number of connected components in the underlying graph.

When both  $\|\Delta\beta_0\|_1 = O(1)$  and  $\text{nullity}(\Delta) = O(1)$ , Theorem 3 says that the estimate  $\hat{\beta}$  converges in average squared error at the rate  $M\sqrt{\log r}/n$ , in probability. This theorem is quite general, as it applies to any linear operator  $\Delta$ , and one might hence think that it cannot yield sharp rates. Still, as we show next, it does imply consistency for graph trend filtering in certain cases.

**Corollary 4.** *Consider the trend filtering estimator  $\hat{\beta}$  of order  $k$ , and the choice of the tuning parameter  $\lambda$  as in Theorem 3. Then:*

1. *for univariate trend filtering (i.e., essentially GTF on a chain graph),*

$$\frac{\|\hat{\beta} - \beta_0\|_2^2}{n} = O_{\mathbb{P}} \left( \sqrt{\frac{\log n}{n}} \cdot n^k \|\Delta^{(k+1)}\beta_0\|_1 \right);$$

2. *for GTF on an Erdos-Renyi random graph, with edge probability  $p$ , and expected degree  $d = np \geq 1$ ,*

$$\frac{\|\hat{\beta} - \beta_0\|_2^2}{n} = O_{\mathbb{P}} \left( \frac{\sqrt{\log(nd)}}{nd^{\frac{k+1}{2}}} \cdot \|\Delta^{(k+1)}\beta_0\|_1 \right);$$

3. *for GTF on a Ramanujan  $d$ -regular graph, and  $d \geq 1$ ,*

$$\frac{\|\hat{\beta} - \beta_0\|_2^2}{n} = O_{\mathbb{P}} \left( \frac{\sqrt{\log(nd)}}{nd^{\frac{k+1}{2}}} \cdot \|\Delta^{(k+1)}\beta_0\|_1 \right).$$

Cases 2 and 3 of Corollary 4 stem from the simple inequality  $M \leq \|\Delta^\dagger\|_2$ , the largest singular value of  $\Delta^\dagger$ . When  $\Delta = \Delta^{(k+1)}$ , the GTF operator of order  $k+1$ , we have  $\|(\Delta^{(k+1)})^\dagger\|_2 \leq 1/\lambda_{\min}(L)^{(k+1)/2}$ , where  $\lambda_{\min}(L)$  is the smallest nonzero eigenvalue of the Laplacian  $L$  (also known as the Fiedler value [14]). In general,  $\lambda_{\min}(L)$  can be very small, leading to loose error bounds, but for the particular graphs in question, it is well-controlled. When  $\|\Delta^{(k+1)}\beta_0\|_1$  is bounded, cases 2 and 3 of the corollary show that the average squared error of GTF converges at the rate  $\sqrt{\log(nd)}/(nd^{(k+1)/2})$ . As  $k$  increases, this rate is stronger, but so is the assumption that  $\|\Delta^{(k+1)}\beta_0\|_1$  is bounded.

Case 1 in Corollary 4 covers univariate trend filtering (which, recall, is basically the same as GTF over a chain graph; the only differences between the two are boundary terms in the construction of the difference operators). The result in case 1 is based on direct calculation of  $M$ , using specific facts that are known about the univariate difference operators. It is natural in the univariate setting to assume that  $n^k \|\Delta^{(k+1)}\beta_0\|_1$  is

bounded (this is the scaling that would link  $\beta_0$  to the evaluations of a piecewise polynomial function  $f_0$  over  $[0, 1]$ , with  $\text{TV}(f_0^{(k)})$  bounded). Under such an assumption, the above corollary yields a convergence rate of  $\sqrt{\log n/n}$  for univariate trend filtering, which is not tight. A more refined analysis shows the univariate trend filtering estimator to converge at the minimax optimal rate  $n^{-(2k+2)/(2k+3)}$ , proved in [38] by using a connection between univariate trend filtering and locally adaptive regression splines, and relying on sharp entropy-based rates for locally adaptive regression splines from [22].

We note that in a pure graph-centric setting, the latter strategy is not generally applicable, as the notion of a spline function does not obviously extend to the nodes of an arbitrary graph structure. In a later subsection, we derive fast error rates for GTF based directly on entropy bounds for the unit ball under the GTF regularizer. In principle, this completely circumvents the need for a connection to splines, and is applicable to trend filtering over arbitrary graphs. As an important verification for the strength of this approach, we show that it can be used to recover the optimal rates of convergence for univariate trend filtering. Before this, we study fast error rates for GTF that follow from a different framework, based on incoherence.

## 6.2 Strong Error Bounds Based on Incoherence

A key step in the proof of Theorem 3 argues, roughly speaking, that

$$\epsilon^\top \Delta^\dagger \Delta x \leq \|(\Delta^\dagger)^\top \epsilon\|_\infty \|\Delta x\|_1 = O_{\mathbb{P}}(M\sqrt{\log r} \|\Delta x\|_1), \quad (14)$$

where  $\epsilon \sim \mathcal{N}(0, \sigma^2 I)$ . The second bound holds by a standard result on maxima of Gaussians (recall that  $M$  is largest  $\ell_2$  norm of the columns of  $\Delta^\dagger$ ). The first bound above uses Holder's inequality; note that this applies to any  $\epsilon, \Delta$ , i.e., it does not use any information about the distribution of  $\epsilon$ , or the properties of  $\Delta$ . The next lemma reveals a potential advantage that can be gained from replacing the bound (14), stemming from Holder's inequality, with a "linearized" bound.

**Lemma 5.** *Denote  $\epsilon \sim \mathcal{N}(0, \sigma^2 I)$ , and assume that*

$$\max_{x \in \mathcal{S}_\Delta(1)} \frac{\epsilon^\top x - A}{\|x\|_2} = O_{\mathbb{P}}(B), \quad (15)$$

where  $\mathcal{S}_\Delta(1) = \{x \in \text{row}(\Delta) : \|\Delta x\|_1 \leq 1\}$ . With  $\lambda = \Theta(A)$ , the generalized lasso estimate  $\hat{\beta}$  satisfies

$$\frac{\|\hat{\beta} - \beta_0\|_2^2}{n} = O_{\mathbb{P}}\left(\frac{\text{nullity}(\Delta)}{n} + \frac{B^2}{n} + \frac{A}{n} \cdot \|\Delta \beta_0\|_1\right).$$

The inequality in (15) is referred to as a "linearized" bound because it implies that for  $x \in \mathcal{S}_\Delta(1)$ ,

$$\epsilon^\top x = O_{\mathbb{P}}(A + B\|x\|_2),$$

and the right-hand side is a linear function of  $\|x\|_2$ . Indeed, for  $A = M\sqrt{2\log r}$  and  $B = 0$ , this encompasses the bound in (14) as a special case, and the result of Lemma 5 reduces to that of Theorem 3. But the result in Lemma 5 can be much stronger, if  $A, B$  can be adjusted so that  $A$  is smaller than  $M\sqrt{2\log r}$ , and  $B$  is also small. Such an arrangement is possible for certain operators  $\Delta$ ; e.g., it is possible under an incoherence-type assumption on  $\Delta$ .

**Theorem 6.** *Let  $\xi_1 \leq \dots \leq \xi_n$  denote the singular values of  $\Delta$ , ordered to be increasing, and let  $\psi_1, \dots, \psi_r$  be the left singular vectors. Assume the incoherence condition:*

$$\|\psi_i\|_\infty \leq \mu/\sqrt{n}, \quad i = 1, \dots, r,$$

for some  $\mu > 0$ . Now let  $i_0 \in \{1, \dots, n\}$ , and let

$$\lambda = \Theta \left( \mu \sqrt{\frac{\log r}{n} \sum_{i=i_0+1}^n \frac{1}{\xi_i^2}} \right).$$

Then the generalized lasso estimate  $\hat{\beta}$  has average squared error

$$\frac{\|\hat{\beta} - \beta_0\|_2^2}{n} = O_{\mathbb{P}} \left( \frac{\text{nullity}(\Delta)}{n} + \frac{i_0}{n} + \frac{\mu}{n} \sqrt{\frac{\log r}{n} \sum_{i=i_0+1}^n \frac{1}{\xi_i^2}} \cdot \|\Delta\beta_0\|_1 \right).$$

Theorem 6 is proved by leveraging the linearized bound (15), which holds under the incoherence condition on the singular vectors of  $\Delta$ . Compared to the basic result in Theorem 3, the result in Theorem 6 is clearly stronger as it allows us to replace  $M$ —which can grow like the reciprocal of the minimum nonzero singular value of  $\Delta$ —with something akin to the average reciprocal of larger singular values. But it does, of course, also make stronger assumptions (incoherence). It is interesting to note that the functional in the theorem,  $\sum_{i=i_0+1}^n \xi_i^{-2}$ , was also determined to play a leading role in error bounds for a graph Fourier based scan statistic in the hypothesis testing framework [29].

Applying the above theorem to the GTF estimator requires knowledge of the singular vectors of  $\Delta = \Delta^{(k+1)}$ , the  $(k+1)$ st order graph difference operator. The validity of an incoherence assumption on these singular vectors depend on the graph  $G$  in question. Graphs that are expected to exhibit the incoherence condition will be regular in the sense in that neighborhoods of different vertices look roughly the same. Social networks are likely to have this property for the bulk of their vertices (i.e., with the exception of a small number of high degree nodes). Another particular graph of this type is the regular 2d torus with  $\ell \times \ell$  vertices. We give a corollary regarding this graph, and the case  $k = 1$ .

**Corollary 7.** *Let  $G$  be a regular square  $\ell \times \ell$  torus, so that  $n = \ell^2$ , and let  $k = 1$ . Then, with the choice  $\lambda = \Theta((\log n)^{2/7} n^{3/7} \cdot \|\Delta\beta_0\|_1^{-3/7})$ , the GTF estimator  $\hat{\beta}$  satisfies*

$$\frac{\|\hat{\beta} - \beta_0\|_2^2}{n} = O_{\mathbb{P}} \left( \frac{(\log n)^{2/7}}{n^{4/7}} \cdot \|\Delta\beta_0\|_1^{4/7} \right).$$

### 6.3 Strong Error Bounds Based on Entropy

A different “fractional” bound on the Gaussian contrast  $\epsilon^\top x$ , over  $x \in \mathcal{S}_\Delta(1)$ , provides an alternate route to deriving sharper rates. This style of bound is inspired by the seminal work of [41].

**Lemma 8.** *Denote  $\epsilon \sim \mathcal{N}(0, \sigma^2 I)$ , and assume that for a constant  $w < 2$ ,*

$$\max_{x \in \mathcal{S}_\Delta(1)} \frac{\epsilon^\top x}{\|x\|_2^{1-w/2}} = O_{\mathbb{P}}(K), \tag{16}$$

where recall  $\mathcal{S}_\Delta(1) = \{x \in \text{row}(\Delta) : \|\Delta x\|_1 \leq 1\}$ . Then with

$$\lambda = \Theta \left( K^{\frac{2}{1+w/2}} \cdot \|\Delta\beta_0\|_1^{-\frac{1-w/2}{1+w/2}} \right),$$

the generalized lasso estimate  $\hat{\beta}$  satisfies

$$\frac{\|\hat{\beta} - \beta_0\|_2^2}{n} = O_{\mathbb{P}} \left( \frac{\text{nullity}(\Delta)}{n} + \frac{K^{\frac{2}{1+w/2}}}{n} \cdot \|\Delta\beta_0\|_1^{\frac{w}{1+w/2}} \right).$$

The main motivation for bounds of the form (16) is that they follow from entropy bounds on the set  $\mathcal{S}_\Delta(1)$ . Recall that for a set  $S$ , the covering number  $N(\delta, S, \|\cdot\|)$  is the fewest number of balls of radius  $\delta$  that cover  $S$ , with respect to the norm  $\|\cdot\|$ . The log covering or entropy number is  $\log N(\delta, S, \|\cdot\|)$ . In the next result, we make the connection between between entropy and fractional bounds precise; this follows closely from Lemma 3.5 of [41].

**Theorem 9.** *Suppose that there exist a constant  $w < 2$  such that for  $n$  large enough,*

$$\log N(\delta, \mathcal{S}_\Delta(1), \|\cdot\|_2) \leq E \left( \frac{\sqrt{n}}{\delta} \right)^w, \quad (17)$$

for  $\delta > 0$ , where  $E$  can depend on  $n$ . Then the fractional bound in (16) holds with  $K = \sqrt{E}n^{w/4}$ , and as a result, for

$$\lambda = \Theta \left( E^{\frac{1}{1+w/2}} n^{\frac{w/2}{1+w/2}} \|\Delta\beta_0\|_1^{-\frac{1-w/2}{1+w/2}} \right),$$

the generalized lasso estimate  $\hat{\beta}$  has average squared error

$$\frac{\|\hat{\beta} - \beta_0\|_2^2}{n} = O_{\mathbb{P}} \left( \frac{\text{nullity}(\Delta)}{n} + E^{\frac{1}{1+w/2}} n^{-\frac{1}{1+w/2}} \cdot \|\Delta\beta_0\|_1^{\frac{w}{1+w/2}} \right).$$

As  $w$  is made smaller in the entropy bound (17), we see that the rate of convergence guaranteed by Theorem 9 becomes faster. To confirm just how sharp these rates can be, we use the theorem to reproduce optimal rates of convergence for univariate trend filtering estimates. In this setting, an entropy bound of the form (17) is easily verified for the univariate operator  $\Delta = D^{(k+1)}$  by appealing to results on entropy in well-studied function spaces.

**Corollary 10.** *Let  $\Delta = D^{(k+1)}$  be the univariate discrete difference operator, of order  $k + 1$ . Then the entropy bound (17) holds with  $w = 1/(k + 1)$  and  $E = n^{k/(k+1)}$ . Hence, with tuning parameter*

$$\lambda = \Theta \left( n^{\frac{2k+1}{2k+3}} \cdot \|D^{(k+1)}\beta_0\|^{-\frac{2k+1}{2k+3}} \right),$$

the univariate trend filtering estimate  $\hat{\beta}$  satisfies

$$\frac{\|\hat{\beta} - \beta_0\|_2^2}{n} = O_{\mathbb{P}} \left( n^{-\frac{2k+2}{2k+3}} \cdot \left( n^k \|D^{(k+1)}\beta_0\|_1 \right)^{\frac{2}{2k+3}} \right).$$

The result of Corollary 10 is written in such a way to convey, as discussed earlier, that it is standard to assume boundedness of  $n^k \|D^{(k+1)}\beta_0\|_1$  in the univariate setting. (The same assumption is made in, e.g., [38, 44], but in each instance, the way it is stated depends on the range of inputs over which the difference operators are defined.) It is evident that for  $n^k \|D^{(k+1)}\beta_0\|_1$  bounded, Corollary 10 shows the univariate trend filtering estimate converges at the rate  $n^{-(2k+2)/(2k+3)}$ , which is known to be minimax optimal, and matches the results in [38, 44]. The proof of the corollary establishes an entropy bound of the form (17) by embedding  $\mathcal{S}_\Delta(1)$  in a larger set that contains (the evaluations of) smooth functions, whose derivatives are of bounded variation. This proof technique, unlike that used in previous works, is free from any dependence on univariate spline functions.<sup>3</sup>

For a general graph, it seems hard to derive entropy bounds on  $\mathcal{S}_\Delta(1)$  in a similar manner, given our (currently) limited understanding of the continuous-time analog of GTF. To be perfectly clear, though, this

<sup>3</sup>To be perfectly fair, the results in [38, 44] are also somewhat broader than that in Corollary 10, in that they do not directly assume boundedness of the underlying signal  $\beta_0$  with respect to the trend filtering regularizer, but instead assume that  $\beta_0$  contains the evaluations of a smooth function  $f_0$  over  $[0, 1]$ , with  $\text{TV}(f_0^{(k)})$  bounded.

difficulty merely concerns the *particular strategy* taken to calculate the entropy number of  $\mathcal{S}_\Delta(1)$ , and not the overall strategy laid out in Theorem 9. The literature on entropy numbers is rich, and there are various methods for computing entropy bounds, any of which can be used for our purposes as long as the bounds fit the form of (17), as required by the theorem. Some common strategies, for bounding the entropy of  $\mathcal{S}_\Delta(1)$ , use either a characterization of the spectral decay of  $\Delta^\dagger$ , an analysis of the correlations between columns of  $\Delta^\dagger$ , or a covering number bound on the columns of  $\Delta^\dagger$ . For a nice display of such strategies and their applications, we refer the reader to Section 6 of [42] and Section 14.12 of [8]. An in-depth study of each of the aforementioned strategies, with regard to GTF, is beyond the scope of this paper, but is a topic for future work. We conclude by demonstrating the capabilities of third strategy: using a very simple covering number argument on the columns of  $\Delta^\dagger$ , we can recover the optimal rate of convergence for the univariate fused lasso.

**Corollary 11.** *Let  $g_1, \dots, g_r$  denote the “atoms” associated with  $\Delta$ , i.e., the columns of  $\Delta^\dagger$ , and let  $\mathcal{G} = \{\pm g_i : i = 1, \dots, r\}$  denote the symmetrized set of atoms. Suppose that there exists constants  $\zeta, C_0$  with the following property: for each  $j = 1, \dots, 2r$ , there is an arrangement of  $j$  balls having radius at most*

$$C_0 \sqrt{n} j^{-1/\zeta},$$

*with respect to the norm  $\|\cdot\|_2$ , that covers  $\mathcal{G}$ . Then the entropy bound in (17) is met with  $w = 2\zeta/(2 + \zeta)$  and  $E = O(1)$ . Therefore, the generalized lasso estimate  $\hat{\beta}$  satisfies the error bound in Theorem 9, with  $\lambda$  also as in this theorem.*

*An easy example concerns the univariate difference operator of first order,  $\Delta = D^{(1)}$ . In this case, the symmetrized set  $\mathcal{G}$  of atoms can be covered by  $j$  balls with radius at most  $\sqrt{2n/j}$ , for  $j = 1, \dots, 2(n - 1)$ . Thus, with  $\lambda = \Theta(n^{1/3} \|D^{(1)}\beta_0\|_1^{-1/3})$ , the univariate fused lasso estimate  $\hat{\beta}$  satisfies*

$$\frac{\|\hat{\beta} - \beta_0\|_2^2}{n} = O_{\mathbb{P}}\left(n^{-2/3} \cdot \|D^{(1)}\beta_0\|_1^{2/3}\right).$$

## 7 Discussion

In this work, we proposed graph trend filtering as a useful alternative to Laplacian and wavelet smoothers on graphs. This is analogous to the usefulness of univariate trend filtering in nonparametric regression, as an alternative to smoothing splines and wavelets [38]. We have documented empirical evidence for the superior local adaptivity of the  $\ell_1$ -based GTF over the  $\ell_2$ -based graph Laplacian smoother, and the superior robustness of GTF over wavelet smoothing in high-noise scenarios. Our theoretical analysis provides a basis for a deeper understanding of the estimation properties of GTF. More precise theoretical characterizations involving entropy will be the topic of future work, as will comparisons between the error rates achieved by GTF and other common estimators, such as Laplacian smoothing. These extensions, and many others, are well within reach.

## Acknowledgments

YW was supported by the Singapore National Research Foundation under its International Research Centre @ Singapore Funding Initiative and administered by the IDM Programme Office. JS was supported by NSF Grant DMS-1223137. AS was supported by a Google Faculty Research Grant. RT was supported by NSF Grant DMS-1309174.

## A Proofs of Theoretical Results

### A.1 Proof of Theorem 3

By assumption we can write

$$y = \beta_0 + \epsilon, \quad \epsilon \sim \mathcal{N}(0, \sigma^2 I).$$

Denote  $R = \text{row}(\Delta)$ , the row space of  $\Delta$ , and  $R^\perp = \text{null}(\Delta)$ , the null space of  $\Delta$ . Also let  $P_R$  be the projection onto  $R$ , and  $P_{R^\perp}$  the projection onto  $R^\perp$ . Consider

$$\begin{aligned} \hat{\beta} &= \operatorname{argmin}_{\beta \in \mathbb{R}^n} \frac{1}{2} \|y - \beta\|_2^2 + \lambda \|\Delta\beta\|_1, \\ \tilde{\beta} &= \operatorname{argmin}_{\beta \in \mathbb{R}^n} \frac{1}{2} \|P_R y - \beta\|_2^2 + \lambda \|\Delta\beta\|_1. \end{aligned}$$

The first quantity  $\hat{\beta} \in \mathbb{R}^n$  is the estimate of interest, the second one  $\tilde{\beta} \in R$  is easier to analyze. Note that

$$\hat{\beta} = P_{R^\perp} y + \tilde{\beta},$$

and write  $\|x\|_R = \|P_R x\|_2$ ,  $\|x\|_{R^\perp} = \|P_{R^\perp} x\|_2$ . Then

$$\|\hat{\beta} - \beta_0\|_2^2 = \|\epsilon\|_{R^\perp}^2 + \|\tilde{\beta} - \beta_0\|_R^2.$$

The first term is on the order  $\dim(R^\perp) = \text{nullity}(\Delta)$ , and it suffices to bound the second term. Now we establish a basic inequality for  $\tilde{\beta}$ . By optimality of  $\tilde{\beta}$ , we have

$$\frac{1}{2} \|y - \tilde{\beta}\|_R^2 + \lambda \|\Delta\tilde{\beta}\|_1 \leq \frac{1}{2} \|y - \beta_0\|_R^2 + \lambda \|\Delta\beta_0\|_1,$$

and after rearranging terms,

$$\|\tilde{\beta} - \beta_0\|_R^2 \leq 2\epsilon^\top P_R (\tilde{\beta} - \beta_0) + 2\lambda \|\Delta\beta_0\|_1 - 2\lambda \|\Delta\tilde{\beta}\|_1. \quad (18)$$

This is our basic inequality. In the first term above, we use  $P_R = \Delta^\dagger \Delta$ , and apply Holder's inequality:

$$\epsilon^\top \Delta^\dagger \Delta (\tilde{\beta} - \beta_0) \leq \|(\Delta^\dagger)^\top \epsilon\|_\infty \|\Delta(\tilde{\beta} - \beta_0)\|_1. \quad (19)$$

If  $\lambda \geq \|(\Delta^\dagger)^\top \epsilon\|_\infty$ , then from (18), (19) we see that

$$\|\tilde{\beta} - \beta_0\|_R^2 \leq 4\lambda \|\Delta\beta_0\|_1.$$

Well,  $\|(\Delta^\dagger)^\top \epsilon\|_\infty = O_{\mathbb{P}}(M\sqrt{\log r})$  by a standard result on the maximum of Gaussians (derived using the union bound, and Mills' bound on the Gaussian tail), where recall  $M$  is the maximum  $\ell_2$  norm of the columns of  $\Delta^\dagger$ . Thus with  $\lambda = \Theta(M\sqrt{\log r})$ , we have from the above that

$$\|\tilde{\beta} - \beta_0\|_R^2 = O_{\mathbb{P}}(M\sqrt{\log r} \|\Delta\beta_0\|_1),$$

as desired.

## A.2 Proof of Corollary 4

**Case 1.** When  $\hat{\beta}$  is the univariate trend filtering estimator of order  $k$ , we are considering a penalty matrix  $\Delta = D^{(k+1)}$ , the univariate difference operator of order  $k+1$ . Note that  $D^{(k+1)} \in \mathbb{R}^{(n-k-1) \times n}$ , and its null space has constant dimension  $k+1$ . We show in Lemma 12 of Appendix A.3 that  $(D^{(k+1)})^\dagger = P_R H_2^{(k)} / k!$ , where  $R = \text{row}(D^{(k+1)})$ , and  $H_2^{(k)} \in \mathbb{R}^{n \times (n-k-1)}$  contains the last  $n-k-1$  columns of the order  $k$  falling factorial basis matrix [44], evaluated over the input points  $x_1 = 1, \dots, x_n = n$ . The largest column norm of  $P_R H_2^{(k)} / k!$  is on the order of  $n^{k+1/2}$ , which proves the result.

**Cases 2 and 3.** When  $G$  is the Ramanujan  $d$ -regular graph, the number of edges in the graph is  $O(nd)$ . The operator  $\Delta = \Delta^{(k+1)}$  has number of rows  $r = n$  when  $k$  is odd and  $r = O(nd)$  when  $k$  is even; overall this is  $O(nd)$ . The dimension of the null space of  $\Delta$  is constant (it is in fact 1, since the graph is connected). When  $G$  is the Erdos-Renyi random graph, the same bounds apply to the number of rows and the dimension of the null space, except that the bounds become probabilistic ones.

Now we apply the crude inequality

$$M = \max_{i=1, \dots, r} \Delta^\dagger e_i \leq \max_{\|x\|_2 \leq 1} \Delta^\dagger x = \|\Delta^\dagger\|_2,$$

the right-hand side being the maximum singular value of  $\Delta^\dagger$ . As  $\Delta = \Delta^{(k+1)}$ , the graph difference operator of order  $k+1$ , we claim that

$$\|\Delta^\dagger\|_2 \leq 1 / \lambda_{\min}(L)^{\frac{k+1}{2}}, \quad (20)$$

where  $\lambda_{\min}(L)$  denotes the smallest nonzero eigenvalue of the graph Laplacian  $L$ . To see this, note first that  $\|\Delta^\dagger\|_2 = 1 / \sigma_{\min}(\Delta)$ , where the denominator is the smallest nonzero singular value of  $\Delta$ . Now for odd  $k$ , we have  $\Delta^{(k+1)} = L^{(k+1)/2}$ , and the claim follows as

$$\sigma_{\min}(L^{\frac{k+1}{2}}) = \min_{x \in R: \|x\|_2 \leq 1} L^{\frac{k+1}{2}} x \geq (\sigma_{\min}(L))^{\frac{k+1}{2}},$$

and  $\sigma_{\min}(L) = \lambda_{\min}(L)$ , since  $L$  is symmetric. Above,  $R$  denotes the row space of  $L$  (the space orthogonal to the vector  $\mathbb{1}$  of all 1s). For even  $k$ , we have  $\Delta^{(k+1)} = DL^{k/2}$ , and again

$$\sigma_{\min}(DL^{\frac{k}{2}}) = \min_{x \in R: \|x\|_2 \leq 1} DL^{\frac{k}{2}} x \geq \sigma_{\min}(D) (\sigma_{\min}(L))^{\frac{k}{2}},$$

where  $\sigma_{\min}(D) = \sqrt{\lambda_{\min}(L)}$ , since  $D^\top D = L$ . This verifies the claim.

Having established (20), it suffices to lower bound  $\lambda_{\min}(L)$  for the two graphs in question. Indeed, for both graphs, we have the lower bound

$$\lambda_{\min}(L) = \Omega(d - \sqrt{d}).$$

e.g., see [20, 23] for the Ramanujan graph and [13, 11] for the Erdos-Renyi graph. This completes the proof.

## A.3 Calculation of $(D^{(k+1)})^\dagger$

**Lemma 12.** *The  $(k+1)$ st order discrete difference operator has pseudoinverse  $(D^{(k+1)})^\dagger = P_R H_2^{(k)} / k!$ , where we denote  $R = \text{row}(D^{(k+1)})$ , and  $H_2^{(k)} \in \mathbb{R}^{n \times (n-k-1)}$  the last  $n-k-1$  columns of the  $k$ th order falling factorial basis matrix.*

*Proof.* We abbreviate  $D = D^{(k+1)}$ , and consider the linear system

$$DD^\top x = Db \quad (21)$$

in  $x$ , where  $b \in \mathbb{R}^n$  is arbitrary. We seek an expression for  $x = (DD^\top)^{-1}D^\top = (D^\dagger)^\top b$ , and this will tell us the form of  $D^\dagger$ . Define

$$\tilde{D} = \begin{bmatrix} C \\ D \end{bmatrix} \in \mathbb{R}^{n \times n},$$

where  $C \in \mathbb{R}^{(k+1) \times n}$  is the matrix that collects the first row of each lower order difference operator, defined in Lemma 2 of [44]. From this same lemma, we know that

$$\tilde{D}^{-1} = H/k!,$$

where  $H = H^{(k)}$  is falling factorial basis matrix of order  $k$ , evaluated over  $x_1, \dots, x_n$ . With this in mind, consider the expanded linear system

$$\begin{bmatrix} CC^\top & CD^\top \\ DC^\top & DD^\top \end{bmatrix} \begin{bmatrix} w \\ x \end{bmatrix} = \begin{bmatrix} a \\ Db \end{bmatrix}. \quad (22)$$

The second equation reads

$$DC^\top w + DD^\top x = Db,$$

and so if we can choose  $a$  in (22) so that at the solution we have  $w = 0$ , then  $x$  is the solution in (21). The first equation in (22) reads

$$CC^\top w + CD^\top x = a,$$

i.e.,

$$w = (CC^\top)^{-1}(CD^\top x - a).$$

That is, we want to choose

$$a = CD^\top x = CD^\top (DD^\top)^{-1}Db = CP_R b,$$

where  $P_R$  is the projection onto row space of  $D$ . Thus we can reexpress (22) as

$$\tilde{D}\tilde{D}^\top \begin{bmatrix} w \\ x \end{bmatrix} = \begin{bmatrix} CP_R b \\ Db \end{bmatrix} = \tilde{D}P_R b$$

and, using  $\tilde{D}^{-1} = H/k!$ ,

$$\begin{bmatrix} w \\ x \end{bmatrix} = H^\top P_R b / k!.$$

Finally, writing  $H_2$  for the last  $n - k - 1$  columns of  $H$ , we have  $x = H_2^\top P_R b / k!$ , as desired.  $\square$

*Remark.* The above proof did not rely on the input points  $x_1, \dots, x_n$ ; indeed, the result holds true for any sequence of inputs used to define the discrete difference matrix and falling factorial basis matrix.

#### A.4 Proof of Lemma 5

We follow the proof of Theorem 3, up until the application of Holder's inequality in (19). In place of this step, we use the linearized bound in (15), which we claim implies that

$$\epsilon^\top P_R(\tilde{\beta} - \beta_0) \leq \tilde{B}\|\tilde{\beta} - \beta_0\|_R + A\|\Delta(\tilde{\beta} - \beta_0)\|_1,$$

where  $\tilde{B} = O_{\mathbb{P}}(B)$ . This simply follows from applying (15) to  $x = P_R(\tilde{\beta} - \beta_0) / \|\Delta(\tilde{\beta} - \beta_0)\|_1$ , which is easily seen to be an element of  $\mathcal{S}_\Delta(1)$ . Hence we can take  $\lambda = \Theta(A)$ , and argue as in the proof of Theorem 3 to arrive at

$$\|\tilde{\beta} - \beta_0\|_R^2 \leq \tilde{B}\|\tilde{\beta} - \beta_0\|_R + \tilde{A}\|\Delta\beta_0\|_1,$$



where  $\tilde{A} = O_{\mathbb{P}}(A)$ . The above is a quadratic inequality of the form  $ax^2 - bx - c \leq 0$  in  $x = \|\tilde{\beta} - \beta_0\|_R$ . As  $a > 0$ , the larger of its two roots serves as a bound for  $x$ , i.e.,  $x \leq (b + \sqrt{b^2 + 4ac})/(2a) \leq b/a + \sqrt{c/a}$ , or  $x^2 \leq 2b^2/a^2 + 2c/a$ , which means that

$$\|\tilde{\beta} - \beta_0\|_R^2 \leq 2\tilde{B}^2 + 2\tilde{A}\|\Delta\beta_0\|_1 = O_{\mathbb{P}}(B^2 + A\|\Delta\beta_0\|_1),$$

completing the proof.

## A.5 Proof of Theorem 6

For an index  $i_0 \in \{1, \dots, n\}$ , let

$$C = \mu \sqrt{\frac{2 \log 2r}{n} \sum_{i=i_0+1}^n \frac{1}{\xi_i^2}}.$$

We will show that

$$\max_{x \in \mathcal{S}_{\Delta}(1)} \frac{\epsilon^\top x - 1.001\sigma C}{\|x\|_2} = O_{\mathbb{P}}(\sqrt{i_0}).$$

Invoking Lemma 5 would then give the result.

Henceforth we define for a scalar  $a$  the pseudoinverse to be  $a^\dagger = 1/a$  for  $a \neq 0$  and 0 otherwise. We also denote  $[i] = \{1, \dots, i\}$ . Let the singular value decomposition of  $\Delta$  be

$$\Delta = \Psi \Xi \Phi^\top,$$

where  $\Psi \in \mathbb{R}^{r \times r}$ ,  $\Phi \in \mathbb{R}^{n \times n}$  are orthogonal, and  $\Xi \in \mathbb{R}^{r \times n}$  has diagonal elements  $(\Xi)_{ii} = \xi_i$  for  $i \in [n]$ . First, let us establish that

$$\Delta^\dagger = \Phi \Xi^\dagger \Psi^\top,$$

where  $\Xi^\dagger \in \mathbb{R}^{n \times r}$  and  $(\Xi^\dagger)_{ii} = \xi_i^\dagger$  for  $i \in [n]$ . Consider an arbitrary point  $x = P_R z \in \mathcal{S}_{\Delta}(1)$ . Denote the projection  $P_{i_0} = \Phi_{[i_0]} \Phi_{[i_0]}^\top$  where  $\Phi_{[i_0]}$  contains the first  $i_0$  right singular vectors. We can decompose

$$\epsilon^\top P_R z = \epsilon^\top P_{i_0} P_R z + \epsilon^\top (I - P_{i_0}) P_R z.$$

The first term can be bounded by

$$\epsilon^\top P_{i_0} P_R z \leq \|P_{i_0} \epsilon\|_2 \|z\|_R = O_{\mathbb{P}}(\sqrt{i_0} \|z\|_R),$$

using the fact that  $\|P_{i_0} \epsilon\|_2^2 \stackrel{d}{=} \sum_{i=1}^{i_0} \epsilon_i^2$ . We can bound the second term by

$$\epsilon^\top (I - P_{i_0}) P_R z = \epsilon^\top (I - P_{i_0}) \Delta^\dagger \Delta z \leq \|(\Delta^\dagger)^\top (I - P_{i_0}) \epsilon\|_\infty,$$

using  $P_R = \Delta^\dagger \Delta$ , Holder's inequality, and the fact that  $\|\Delta z\|_1 \leq 1$ . Define  $g_j = (I - P_{i_0}) \Delta^\dagger e_j$  for  $j \in [r]$  with  $e_j$  the  $j$ th canonical basis vector. So,

$$\|g_j\|_2^2 = \|\Phi_{[n] \setminus [i_0]} \Xi^\dagger \Psi^\top e_j\|_2^2 \leq \frac{\mu^2}{n} \sum_{k=i_0+1}^n (\xi_k^\dagger)^2,$$

by rotational invariance of  $\|\cdot\|_2$  and the incoherence assumption on the columns of  $\Psi$ . By a standard result on maxima of Gaussians,

$$\|(\Delta^\dagger)^\top (I - P_{i_0}) \epsilon\|_\infty = \max_{j \in [r]} |g_j^\top \epsilon| \leq 1.001\sigma \sqrt{2 \log(2r) \frac{\mu^2}{n} \sum_{k=i_0+1}^n (\xi_k^\dagger)^2} = 1.001\sigma C,$$

with probability approaching 1. Putting the two terms together completes the proof, as we have shown that

$$\frac{\epsilon^\top P_R z - 1.001\sigma C}{\|z\|_R} = O_{\mathbb{P}}(\sqrt{i_0}).$$

## A.6 Proof of Corollary 7

We can associate to every vertex in the torus a pair  $i_1, i_2 \in [\ell] \times [\ell]$ . Recall that  $\Delta$  in this context is the combinatorial Laplacian  $L$ . It can be shown that the eigenvalues and eigenvectors of  $\Delta$  associated with the pair are

$$2(2 - \cos(2\pi i_1) - \cos(2\pi i_2)), N_\ell^{-2}(\sin(2\pi k_1 i_1/\ell))_{k_1 \in [\ell]} \otimes (\sin(2\pi k_2 i_2/\ell))_{k_2 \in [\ell]} = \psi_{(i_1, i_2)},$$

where  $N_\ell$  is a normalizing constant forcing the eigenvectors to be of unit norm. Due to this constraint, we see  $N_\ell \sim \sqrt{\ell}$  (where  $a \sim b$  indicates that  $a = b(1 + o(1))$ ), and we have that

$$\|\psi_{(i_1, i_2)}\|_\infty \sim n^{-1/2},$$

uniformly, and so it obeys the coherence condition with  $\mu$  arbitrarily close to 1 for  $n$  large enough. The remainder of this proof comes from [31], but it is included for completeness. Now, we turn to calculating the functional  $\sum_{i=i_0+1}^n \xi_i^{-2}$ . For  $i \in [\ell]$ , we have  $|\{(i_1, i_2) : i_1 \vee i_2 = i\}| \leq 2i$  and we know that  $\xi_{i_1, i_2} \geq 2(1 - \cos(2\pi i_1 \vee i_2/\ell))$ . Letting  $j_0 \in [\ell]$  such that  $j_0 = o(\ell)$ , then

$$\begin{aligned} \frac{1}{n} \sum_{i_1 \vee i_2 > j_0} \frac{1}{\xi_{i_1, i_2}^2} &\leq \frac{1}{n} \sum_{j=j_0}^{\ell} \frac{2j}{(2(1 - \cos(2\pi j/\ell)))^2} \\ &\leq \frac{1}{2\ell} \sum_{j=j_0}^{\ell} \frac{j/\ell}{(1 - \cos(2\pi j/\ell))^2} \\ &\sim \frac{1}{2} \int_{j_0/\ell}^1 \frac{x}{(1 - \cos(2\pi x))^2} dx \sim \frac{1}{2} \left(\frac{\ell}{j_0}\right)^3, \end{aligned}$$

by a Taylor expansion about  $x = 0$ . Moreover,  $i_0 = |\{(i_1, i_2 \in [\ell] : i_1 \vee i_2 \leq j_0)\}| = j_0^2$  and so we will seek to balance  $i_0 = j_0^2$  with  $\sqrt{(\log n)\ell^3/j_0^3} \cdot \|\Delta\beta_0\|_1$ . This is accomplished by

$$j_0 \sim (\log n)^{1/7} n^{3/14} \cdot \|\Delta\beta_0\|_1^{2/7}.$$

Applying Theorem 6 gives us our result.

## A.7 Proof of Lemma 8

As before, we follow the proof of Theorem 3 up until the application of Holder's inequality in (19), but we use the fractional bound in (16) instead. We claim that this implies

$$\epsilon^\top P_R(\tilde{\beta} - \beta_0) \leq \tilde{K} \|\tilde{\beta} - \beta_0\|_R^{1-w/2} (\|\Delta\tilde{\beta}\|_1 + \|\Delta\beta_0\|_1)^{w/2},$$

where  $\tilde{K} = O_{\mathbb{P}}(K)$ . This is verified by noting that  $x = P_R(\tilde{\beta} - \beta_0)/(\|\Delta\tilde{\beta}\|_1 + \|\Delta\beta_0\|_1) \in \mathcal{S}_\Delta(1)$ , applying (16) to  $x$ , and then rearranging. Therefore, as in the proof of Theorem 3, we have

$$\|\tilde{\beta} - \beta_0\|_R^2 \leq 2\tilde{K} \|\tilde{\beta} - \beta_0\|_R^{1-w/2} (\|\Delta\tilde{\beta}\|_1 + \|\Delta\beta_0\|_1)^{w/2} + 2\lambda(\|\Delta\beta_0\|_1 - \|\Delta\tilde{\beta}\|_1), \quad (23)$$

We now set

$$\lambda = \Theta \left( K \frac{2}{1+w/2} \|\Delta\beta_0\|_1^{-\frac{1-w/2}{1+w/2}} \right),$$

and in the spirit of [41, 22], we proceed to argue in cases.

**Case 1.** Suppose that  $\frac{1}{2}\|\Delta\tilde{\beta}\|_1 \geq \|\Delta\beta_0\|_1$ . Then we see that (23) implies

$$0 \leq \|\tilde{\beta} - \beta_0\|_R^2 \leq \tilde{K}\|\tilde{\beta} - \beta_0\|_R^{1-w/2} \left(\frac{3}{2}\right)^{w/2} \|\Delta\tilde{\beta}\|_1^{w/2} - \lambda\|\Delta\tilde{\beta}\|_1, \quad (24)$$

so that

$$\lambda\|\Delta\tilde{\beta}\|_1 \leq \tilde{K}\|\tilde{\beta} - \beta_0\|_R^{1-w/2} \|\Delta\tilde{\beta}\|_1^{w/2},$$

where for simplicity have absorbed a constant factor  $2(3/2)^{w/2}$  into  $\tilde{K}$  (since this does not change the fact that  $\tilde{K} = O_{\mathbb{P}}(K)$ ), and thus

$$\|\Delta\tilde{\beta}\|_1 \leq \left(\frac{\tilde{K}}{\lambda}\right)^{\frac{1}{1-w/2}} \|\tilde{\beta} - \beta_0\|_R.$$

Plugging this back into (24) gives

$$\|\tilde{\beta} - \beta_0\|_R^2 \leq \tilde{K}\|\tilde{\beta} - \beta_0\|_R^{1-w/2} \left(\frac{\tilde{K}}{\lambda}\right)^{\frac{w/2}{1-w/2}} \|\tilde{\beta} - \beta_0\|_R^{w/2},$$

or

$$\|\tilde{\beta} - \beta_0\|_R \leq \tilde{K}^{\frac{1}{1+w/2}} \left(\frac{1}{\lambda}\right)^{\frac{w/2}{1-w/2}} = O_{\mathbb{P}}\left(K^{\frac{1}{1+w/2}} \|\Delta\beta_0\|_1^{\frac{w/2}{1+w/2}}\right),$$

as desired.

**Case 2.** Suppose that  $\frac{1}{2}\|\Delta\tilde{\beta}\|_1 \leq \|\Delta\beta_0\|_1$ . Then from (23),

$$\|\tilde{\beta} - \beta_0\|_R^2 \leq \underbrace{2\lambda\|\Delta\beta_0\|_1}_a + \underbrace{2\tilde{K}\|\tilde{\beta} - \beta_0\|_R^{1-w/2} 3^{w/2} \|\Delta\beta_0\|_1^{w/2}}_b,$$

and hence either  $\|\tilde{\beta} - \beta_0\|_R^2 \leq 2a$ , or  $\|\tilde{\beta} - \beta_0\|_R^2 \leq 2b$ , and  $a \leq b$ . The first subcase is straightforward and leads to

$$\|\tilde{\beta} - \beta_0\|_R \leq 2\sqrt{\lambda\|\Delta\beta_0\|_1} = O_{\mathbb{P}}\left(K^{\frac{1}{1+w/2}} \|\Delta\beta_0\|_1^{\frac{w/2}{1+w/2}}\right),$$

as desired. In the second subcase, we have by assumption

$$\|\tilde{\beta} - \beta_0\|_R^2 \leq 2\tilde{K}\|\tilde{\beta} - \beta_0\|_R^{1-w/2} \|\Delta\beta_0\|_1^{w/2}, \quad (25)$$

$$2\lambda\|\Delta\beta_0\|_1 \leq \tilde{K}\|\tilde{\beta} - \beta_0\|_R^{1-w/2} \|\Delta\beta_0\|_1^{w/2}, \quad (26)$$

where again we have absorbed a constant factor  $2(3^{w/2})$  into  $\tilde{K}$ . Working from (26), we derive

$$\|\Delta\beta_0\|_1 \leq \left(\frac{\tilde{K}}{2\lambda}\right)^{\frac{1}{1-w/2}} \|\tilde{\beta} - \beta_0\|_R,$$

and plugging this back into (25), we see

$$\|\tilde{\beta} - \beta_0\|_R^2 \leq 2\tilde{K}\|\tilde{\beta} - \beta_0\|_R^{1-w/2} \left(\frac{\tilde{K}}{2\lambda}\right)^{\frac{w/2}{1-w/2}} \|\tilde{\beta} - \beta_0\|_R^{w/2},$$

and finally

$$\|\tilde{\beta} - \beta_0\|_R \leq 2\tilde{K}^{\frac{1}{1+w/2}} \left(\frac{1}{\lambda}\right)^{\frac{w/2}{1-w/2}} = O_{\mathbb{P}}\left(K^{\frac{1}{1+w/2}} \|\Delta\beta_0\|_1^{\frac{w/2}{1+w/2}}\right).$$

This completes the second case, and the proof.

## A.8 Proof of Theorem 9

The proof follows closely from Lemma 3.5 of [41]. However, this author uses a different problem scaling than ours, so some care must be taken in applying the lemma. First we abbreviate  $\mathcal{S} = \mathcal{S}_\Delta(1)$ , and define  $\tilde{\mathcal{S}} = \mathcal{S} \cdot \sqrt{n}/M$ , where recall  $M$  is the maximum column norm of  $\Delta^\dagger$ . Now it is not hard to check that

$$\mathcal{S} = \{x \in \text{row}(\Delta) : \|\Delta x\|_1 \leq 1\} = \Delta^\dagger \{\alpha : \|\alpha\|_1 \leq 1\},$$

so that  $\max_{x \in \mathcal{S}} \|x\|_2 \leq M$ , and  $\max_{x \in \tilde{\mathcal{S}}} \|x\|_2 \leq \sqrt{n}$ . This is important because Lemma 3.5 of [41] concerns a form of “local” entropy that allows for deviations on the order of  $\sqrt{n}$  in the norm  $\|\cdot\|_2$ , or equivalently, constant order in the scaled metric  $\|\cdot\|_n = \|\cdot\|_2/\sqrt{n}$ . Hence, the entropy bound in (17) translates into

$$\log N(\delta, \tilde{\mathcal{S}}, \|\cdot\|_2) \leq E \left( \frac{\sqrt{n}}{M} \right)^w \left( \frac{\sqrt{n}}{\delta} \right)^w,$$

that is,

$$\log N(\delta, \tilde{\mathcal{S}}, \|\cdot\|_n) \leq E \left( \frac{\sqrt{n}}{M} \right)^w \delta^{-w}.$$

Now we apply Lemma 3.5 of [41]: in the scaled metric used by this author,

$$\max_{x \in \tilde{\mathcal{S}}} \frac{\epsilon^\top x}{\sqrt{n} \|x\|_n^{1-w/2}} = O_{\mathbb{P}} \left( \sqrt{E} \left( \frac{\sqrt{n}}{M} \right)^{w/2} \right),$$

that is,

$$\max_{x \in \tilde{\mathcal{S}}} \frac{\epsilon^\top x}{\|x\|_2^{1-w/2}} = O_{\mathbb{P}} \left( \sqrt{E} (\sqrt{n})^{w/2} \left( \frac{\sqrt{n}}{M} \right)^{w/2} \right),$$

and finally,

$$\max_{x \in \mathcal{S}} \frac{\epsilon^\top x}{\|x\|_2^{1-w/2}} = O_{\mathbb{P}} \left( \sqrt{E} (\sqrt{n})^{w/2} \right),$$

as desired.

## A.9 Proof of Corollary 10

Abbreviate  $D = D^{(k+1)}$  for the univariate difference operator of order  $k+1$ , and  $\mathcal{S} = \mathcal{S}_D(1)$ . As defined in Section 2.1, the operator  $D$  pertains to the unit spaced input points  $x_1 = 1, \dots, x_n = n$ , and hence for consistency we will stick to this case as well. We note that, with the appropriate modifications, this proof can be made to cover arbitrary inputs  $x_1, \dots, x_n$ . Observe that

$$\mathcal{S} = \{\beta \in \text{row}(D) : \|D\beta\|_1 \leq 1\} = D^\dagger \{\alpha : \|\alpha\|_1 \leq 1\} = \frac{1}{k!} P_k^\perp H \{\alpha : \|\alpha\|_1 \leq 1\},$$

where in the last line we used the explicit form  $D^\dagger = P_k^\perp H/k!$  derived in Lemma 12, where  $H$  denotes the last  $n-k-1$  columns of the falling factorial basis matrix of order  $k$ , and  $P_k^\perp$  is the orthogonal projection onto the space spanned by the first  $k$  polynomial vectors (i.e., the first  $k$  polynomial functions evaluated over the input points). The right-hand side above suggests a natural continuous-time analog for  $\mathcal{S}$ . Denote by  $h_{k+2}, \dots, h_n : [0, 1] \rightarrow \mathbb{R}$  the last  $n-k-1$  falling factorial functions of order  $k$ , whose domain has been scaled down to  $[0, 1]$ , and define the set

$$\mathcal{H} = P_k^\perp \{f \in \text{span}\{h_{k+2}, \dots, h_n\} : \text{TV}(f^{(k)}) \leq 1\},$$

where  $P_k^\perp$  now denotes the projection orthogonal to the first  $k$  polynomial functions, defined with respect to the empirical inner product  $\langle f, g \rangle = \sum_{i=1}^n f(i/n)g(i/n)$ . It follows from the analysis of falling factorial functions [44] that for  $f \in \text{span}\{h_{k+2}, \dots, h_n\}$ , and  $\beta = (f(1/n), f(2/n), \dots, f(1))$  containing the evaluations of  $f$ , we have the relationship  $\text{TV}(f^{(k)}) = n^k \|D\beta\|_1$ . This means, that with respect to the empirical norm given by  $d_e(f) = \langle f, f \rangle^{1/2}$ , we have the entropy number equivalence

$$\log N(\delta, \mathcal{S}, \|\cdot\|_2) = \log N(\delta/n^k, \mathcal{H}, d_e), \quad (27)$$

and therefore it suffices to pursue an entropy bound on the function space  $\mathcal{H}$ . To this end, consider the set

$$\mathcal{F}(\ell, R, T) = \left\{ f : f \text{ is } \ell \text{ times continuously differentiable, } \int_0^1 |f^{(\ell)}(x)| dx \leq R, d_\infty(f) \leq T \right\},$$

where in the above, all functions are assumed to have domain  $[0, 1]$ , and  $d_\infty(f) = \sup_{x \in [0,1]} |f(x)|$  is the sup norm. According to results in [5, 1] (paraphrased in [21]),

$$\log N(\delta, \mathcal{F}(\ell, R, T), d_2) \leq C_0 \left(\frac{R}{\delta}\right)^{1/\ell} + \ell \log \left(\frac{T}{\delta}\right) \quad \text{if } \ell = 1, \quad (28)$$

$$\log N(\delta, \mathcal{F}(\ell, R, T), d_\infty) \leq C_1 \left(\frac{R}{\delta}\right)^{1/\ell} + \ell \log \left(\frac{T}{\delta}\right) \quad \text{if } \ell \geq 2, \quad (29)$$

where  $C_0, C_1$  are constants, and  $d_2(f) = (\int_0^1 f^2(x) dx)^{1/2}$ . Now define the larger space

$$\tilde{\mathcal{F}}(\ell, R, T) = \left\{ f : f \text{ is } \ell \text{ times continuously differentiable, except possibly at } 1/n, 2/n, \dots, 1, \right. \\ \left. \text{TV}(f^{(\ell-1)}) \leq R, d_\infty(f) \leq T \right\}.$$

Because  $\mathcal{F}(\ell, R, T)$  is dense in  $\tilde{\mathcal{F}}(\ell, R, T)$ , with respect to either norm  $d_\infty$  or  $d_2$ , the same entropy bounds in (28), (29) apply to the latter function space. Furthermore, by construction, we have  $\mathcal{H} \subseteq \tilde{\mathcal{F}}(k+1, 1, T_0)$  for a constant  $T_0$ , and hence the entropy bounds in (28), (29) apply to  $\mathcal{H}$  with  $\ell = k+1$  and  $R, T$  both constants. Note that (28) applies to the case  $k=0$ , and (29) to the case  $k \geq 1$ . In either case, these bounds imply that

$$\log N(\delta, \mathcal{H}, d_e) \leq C' \left(\frac{\sqrt{n}}{\delta}\right)^{\frac{1}{k+1}},$$

for a constant  $C'$ , where we have used the fact that  $d_e(f) = \sqrt{n}d_2(f)$  for step functions  $f$  having break points at  $1/n, 2/n, \dots, 1$ , and  $d_e(f) \leq \sqrt{n}d_\infty(f)$  for generic functions  $f$ . Thus we conclude, recalling the entropy relationship between  $\mathcal{S}$  and  $\mathcal{H}$  in (27), that

$$\log N(\delta, \mathcal{S}, \|\cdot\|_2) \leq C'_1 n^{\frac{k}{k+1}} \left(\frac{\sqrt{n}}{\delta}\right)^{\frac{1}{k+1}}.$$

This proves the main content of the corollary. The rest of the statements are obtained by simply reading off the result of Theorem 9 with  $w = 1/(k+1)$  and  $E = n^{k/(k+1)}$ .

## A.10 Proof of Corollary 11

For each  $j = 1, \dots, 2r$ , if  $\mathcal{G}$  is covered by  $j$  balls having radius at most  $C_0 \sqrt{n} j^{-1/\zeta}$ , with respect to the norm  $\|\cdot\|_2$ , then it is covered by  $j$  balls having radius at most  $C_0 j^{-1/\zeta}$ , with respect to the scaled norm  $\|\cdot\|_n = \|\cdot\|_2 / \sqrt{n}$ . By Theorem 1 of [9], this implies that for each  $j = 1, 2, 3, \dots$ , the convex hull  $\text{conv}(\mathcal{G})$

is covered by  $2^j$  balls having radius at most  $C'_0 j^{-(1/2+1/\zeta)}$ , with respect to  $\|\cdot\|_n$ , for another constant  $C'_0$ . Converting this back to an entropy bound in our original metric, and noting that  $\text{conv}(\mathcal{G}) = \mathcal{S}_\Delta(1)$ , we have

$$\log(\delta, \mathcal{S}_\Delta(1), \|\cdot\|_2) \leq C''_0 \left( \frac{\sqrt{n}}{\delta} \right)^{\frac{1}{1/2+1/\zeta}},$$

for a constant  $C''_0$ , as needed. This proves the first part of the corollary.

Secondly, we show the claimed covering number bound when  $\Delta = D^{(1)}$ . According to Lemma 12, we know that  $(D^{(1)})^\dagger = P_1^\perp H$ , where  $H$  is an  $n \times (n-1)$  lower triangular matrix with  $H_{ij} = 1$  if  $i > j$  and 0 otherwise, and  $P_1^\perp$  is the projection map orthogonal to the all 1s vector. Thus  $g_i = P_1^\perp h_i$ ,  $i = 1, \dots, n-1$ , with  $h_1, \dots, h_{n-1}$  denoting the columns of  $H$ . It is immediately apparent that

$$\|g_i - g_\ell\|_2 \leq \|h_i - h_\ell\|_2 \leq \sqrt{i - \ell},$$

for all  $i, \ell$ . Now, given  $2j$  balls at our disposal, consider centering the first  $j$  balls at

$$g_d, g_{2d}, \dots, g_{jd},$$

where  $d = \lfloor n/j \rfloor$ . Also let these balls have radius  $\sqrt{n/j}$ . By construction, then, we see that

$$\|g_1 - g_d\|_2 \leq \sqrt{n/j}, \|g_d - g_{2d}\|_2 \leq \sqrt{n/j}, \dots, \|g_{jd} - g_{n-1}\|_2 \leq \sqrt{n/j},$$

which means that we have covered  $g_1, \dots, g_{n-1}$  with  $j$  balls of radius  $\sqrt{n/j}$ . We can cover  $-g_1, \dots, -g_{n-1}$  with the remaining  $j$  balls analogously. Therefore, we have shown that  $2j$  balls require a radius of  $\sqrt{n/j}$ , or in other words,  $j$  balls require a radius of  $\sqrt{2n/j}$ .

## References

- [1] K. Babenko. *Theoretical Foundations and Construction of Numerical Algorithms for the Problems of Mathematical Physics*. 1979. In Russian.
- [2] A. Barbero and S. Sra. Fast Newton-type methods for total variation regularization. In *Proceedings of the 28th International Conference on Machine Learning (ICML-11)*, pages 313–320, 2011.
- [3] A. Barbero and S. Sra. Modular proximal optimization for multidimensional total-variation regularization. arXiv: 1411.0589, 2014.
- [4] D. P. Bertsekas. Projected Newton methods for optimization problems with simple constraints. *SIAM Journal on Control and Optimization*, 20(2):221–246, 1982.
- [5] M. Birman and M. Solomyak. Piecewise-polynomial approximations of functions of the classes  $w_p^\alpha$ . *Mathematics of the USSR-Sbornik*, 73(115):331–335, 1967. In Russian.
- [6] Y. Boykov and V. Kolmogorov. An experimental comparison of min-cut/max-flow algorithms for energy minimization in vision. *IEEE Trans. on Pattern Analysis and Machine Intelligence*, 26(9): 1124–1137, 2004.
- [7] K. Bredies, K. Kunisch, and T. Pock. Total generalized variation. *SIAM Journal on Imaging Sciences*, 3(3):492–526, 2010.
- [8] P. Buhlmann and S. van de Geer. *Statistics for High-Dimensional Data*. Springer, Berlin, 2011.
- [9] B. Carl. Metric entropy of convex hulls in Hilbert spaces. *Bulletin of the London Mathematical Society*, 29(04):452–458, 1997.
- [10] A. Chambolle and J. Darbon. On total variation minimization and surface evolution using parametric maximum flows. *International journal of computer vision*, 84(3):288–307, 2009.
- [11] F. Chung and M. Radcliffe. On the spectra of general random graphs. *The Electronic Journal of Combinatorics*, 18(1), 2011. #P215.

- [12] H. Doraiswamy, N. Ferreira, T. Damoulas, J. Freire, and C. Silva. Using topological analysis to support event-guided exploration in urban data. *Visualization and Computer Graphics, IEEE Transactions on*, PP(99):1–1, 2014. ISSN 1077-2626. doi: 10.1109/TVCG.2014.2346449.
- [13] U. Feige and E. Ofek. Spectral techniques applied to sparse random graphs. *Random Structures & Algorithms*, 27(2):251–275, 2005.
- [14] M. Fiedler. Algebraic connectivity of graphs. *Czechoslovak Math. J.*, 23(98):298–305, 1973.
- [15] H. Hoefling. A path algorithm for the fused lasso signal approximator. *Journal of Computational and Graphical Statistics*, 19(4):984–1006, 2010.
- [16] J. Kelner, L. Orecchia, A. Sidford, and Z. Zhu. A simple, combinatorial algorithm for solving sdd systems in nearly-linear time. In *Symposium on theory of computing*. ACM, 2013.
- [17] S.-J. Kim, K. Koh, S. Boyd, and D. Gorinevsky.  $\ell_1$  trend filtering. *SIAM Review*, 51(2):339–360, 2009.
- [18] R. Kondor and J. D. Lafferty. Diffusion kernels on graphs and other discrete structures. In *Proc. Intl. Conf. Machine Learning*, pages 315–322, San Francisco, CA, 2002. Morgan Kaufmann.
- [19] I. Koutis, G. L. Miller, and R. Peng. A nearly-m log n time solver for sdd linear systems. In *Foundations of Computer Science (FOCS)*, pages 590–598. IEEE, 2011.
- [20] A. Lubotzky, R. Phillips, and P. Sarnak. Ramanujan graphs. *Combinatorica*, 8(3):261–277, 1988.
- [21] E. Mammen. Nonparametric regression under qualitative smoothness assumptions. *Annals of Statistics*, 19(2):741–759, 1991.
- [22] E. Mammen and S. van de Geer. Locally adaptive regression splines. *Annals of Statistics*, 25(1):387–413, 1997.
- [23] A. W. Marcus, D. A. Spielman, and N. Srivastava. Ramanujan graphs and the solution of the Kadison-Singer problem. arXiv: 1408.4421, 2014.
- [24] J. McAuley and J. Leskovec. Learning to discover social circles in ego networks. *Advances in Neural Information Processing Systems*, 25, 2012.
- [25] A. Ramdas and R. J. Tibshirani. Fast and flexible admm algorithms for trend filtering. arXiv: 1406.2082, 2014.
- [26] L. I. Rudin, S. Osher, and E. Fatemi. Nonlinear total variation based noise removal algorithms. *Physica D: Nonlinear Phenomena*, 60:259–268, 1992.
- [27] S. Setzer, G. Steidl, and T. Teuber. Infimal convolution regularizations with discrete  $\mathbb{H}^1$ -type functionals. *Comm. Math. Sci.*, 9(3):797–872, 2011.
- [28] J. Sharpnack, A. Rinaldo, and A. Singh. Sparsistency via the edge lasso. *International Conference on Artificial Intelligence and Statistics*, 15, 2012.
- [29] J. Sharpnack, A. Rinaldo, and A. Singh. Changepoint detection over graphs with the spectral scan statistic. *arXiv preprint arXiv:1206.0773*, 2012.
- [30] J. Sharpnack, A. Krishnamurthy, and A. Singh. Detecting activations over graphs using spanning tree wavelet bases. *International Conference on Artificial Intelligence and Statistics*, 16, 2013.
- [31] J. Sharpnack, A. Rinaldo, and A. Singh. Detecting anomalous activity on networks with the graph Fourier scan statistic. arXiv: 1311.7217, 2014.
- [32] A. J. Smola and R. Kondor. Kernels and regularization on graphs. In *Conf. Computational Learning Theory*, pages 144–158, 2003.
- [33] D. A. Spielman and S.-H. Teng. Nearly-linear time algorithms for preconditioning and solving symmetric, diagonally dominant linear systems. *arXiv preprint cs/0607105*, 2006.
- [34] G. Steidl, S. Didas, and J. Neumann. Splines in higher order TV regularization. *International Journal of Computer Vision*, 70(3):214–255, 2006.
- [35] P. P. Talukdar and K. Crammer. New regularized algorithms for transductive learning. In *Machine Learning and Knowledge Discovery in Databases*, pages 442–457. Springer, 2009.
- [36] P. P. Talukdar and F. Pereira. Experiments in graph-based semi-supervised learning methods for class-instance acquisition. In *Proceedings of the 48th Annual Meeting of the Association for Computational*

- Linguistics*, pages 1473–1481. Association for Computational Linguistics, 2010.
- [37] R. Tibshirani, M. Saunders, S. Rosset, J. Zhu, and K. Knight. Sparsity and smoothness via the fused lasso. *Journal of the Royal Statistical Society: Series B*, 67(1):91–108, 2005.
  - [38] R. J. Tibshirani. Adaptive piecewise polynomial estimation via trend filtering. *Annals of Statistics*, 42(1):285–323, 2014.
  - [39] R. J. Tibshirani and J. Taylor. The solution path of the generalized lasso. *Annals of Statistics*, 39(3):1335–1371, 2011.
  - [40] R. J. Tibshirani and J. Taylor. Degrees of freedom in lasso problems. *Annals of Statistics*, 40(2):1198–1232, 2012.
  - [41] S. van de Geer. Estimating a regression function. *Annals of Statistics*, 18(2):907–924, 1990.
  - [42] S. van de Geer and J. Lederer. The lasso, correlated design, and improved oracle inequalities. *IMS Collections*, 9:303–316, 2013.
  - [43] N. Vishnoi.  $Lx = b$ : Laplacian solvers and their algorithmic applications. *Foundations and Trends in Theoretical Computer Science*, 8(1–2):1–141, 2012.
  - [44] Y.-X. Wang, A. Smola, and R. J. Tibshirani. The falling factorial basis and its statistical properties. *International Conference on Machine Learning*, 31, 2014.